Advances in photocatalysts based on fullerene C_{60} and its derivatives: Properties, mechanism, synthesis, and applications

Yuan Pan [a,1], Xiaojuan Liu [b,1], Wei Zhang [b,1], Zhifeng Liu [a,*], Guangming Zeng [a,*], Binbin Shao [a], Qinghua Liang [a], Qingyun He [a], Xingzhong Yuan [a], Danlian Huang [a], Ming Chen [a]

[a] College of Environmental Science and Engineering, Hunan University and Key Laboratory of Environmental Biology and Pollution Control (Hunan University), Ministry of Education, Changsha 410082, P.R. China

[b] The First affiliated Hospital of Hunan University of Chinese Medicine, Changsha 410007, China

* Corresponding authors at:

[a] College of Environmental Science and Engineering, Hunan University and Key Laboratory of Environmental Biology and Pollution Control (Hunan University), Ministry of Education, Changsha 410082, P.R. China

E-mail: zhifengliu@hnu.edu.cn (Z. Liu)

E-mail: zgming@hnu.edu.cn (G. Zeng)

[1] The authors contribute equally to this paper.

Abstract

Fullerenes possess high chemical stability, large specific surface area, good electrical conductivity and unique three-dimensional structure. In this paper, we provide a general overview of the latest research results of fullerene-based photocatalysts. Firstly, the current status of semiconductor materials and fullerenes in photocatalytic applications are briefly introduced. Secondly, introduced action mechanisms of photocatalysts modified by fullerene C_{60} and its derivatives, including basic structure, exclusive properties and its effect in photocatalysis and material preparation process. Thirdly, factors affecting material effectiveness and the synthesis strategy of composite photocatalyst modified by fullerene are introduced. Meanwhile, the application advances of the photocatalysts are introduced, including in the degradation of pollutants, organic synthesis, hydrogen production, antibacterial and disinfection in water. Finally, the development trends of fullerenes and their derivatives in photocatalysis are also summarized, including theoretical calculations, the morphological structure control, stable derivatives and increase the selectivity, and new other types of fullerene materials.

Keywords: Fullerenes; Semiconductor photocatalysis; Photocatalytic mechanism; Environmental remediation; Hydrogen production

Contents

1. Introduction

With industrial and commercial development, the world is facing a series of crises, such as energy shortages and environmental problems, which has hindered the further development of human civilization [1, 2]. Researchers have used various methods to deal with these problems and have achieved certain results [3, 4]. As early as 1972, Fujishima and Honda used semiconductor TiO_2 to decompose water under ultraviolet light to produce hydrogen [5]. Inspired by their pioneering work, at present, it is believed that semiconductor photocatalysis to solve these problems is a promising technology. The applications of multiphase photocatalyst based on solar energy and semiconductor have been widely studied, including organic contaminants and harmful bacterial viruses removal, hydrogen production, organic synthesis, reduction of carbon dioxide and so on [6, 7].

Generally, the action of the catalyst mainly involves the following processes: the photocatalyst absorbs solar photons, production and separation of photogenerated electrons and holes in the catalyst and the surface reaction of the catalyst, and photoreactions are sequentially performed in order [8, 9]. In addition, the crystal morphology of the catalyst has a great influence on the degradation activity of the catalyst, its optical properties and chemical properties, and the topographical characteristics of the catalyst surface. The ability to ensure that these factors are at their best is the key to the highest activity of photocatalysts [10]. As far

as we know, semiconductor TiO_2 is the most studied photocatalyst to decompose organic compounds in water and air under ultraviolet light, because of its high reaction efficiency, non-toxicity, good chemical inertness and high cost performance [11-15]. Unfortunately, the wide band gap prevents the TiO_2 photocatalyst from being practical because it can only function under ultraviolet light. However, as far as we know, ultraviolet light accounts for about 4% of the solar spectrum in terms of energy, so most of the solar energy is not used [16]. Consequently, so as to utilize more energy of solar energy, exploring many photocatalysts that can work with visible light has attracted widespread attention. So far, a variety of this type of photocatalysts are being gradually developed and invented, including TiO_2 derivatives ($TiO_{2-x}N_x$ [17] and MIL-125(Ti) derivatives [18]), simple oxides(Bi_2O_3 [19-21], Fe_2O_3[22, 23]and WO_3 [24, 25]), complex oxides ($BiPO_4$ [26, 27], $BiVO_4$ [28, 29], Ag_3PO_4 [30-32]and Bi_2WO_6 [33-35]), metal chalcogenides (CdS [36-38]), and graphitic C_3N_4 [39-41].

Carbon nanomaterials have special properties such as strong physical/chemical stability, excellent electronic properties, limiting effects and developed pore structure [42, 43]. Due to the excellent properties of carbon nanomaterials, they have great practical application value in the field of pollution control [44-48]. Because of these excellent properties, carbon materials (such as graphene, carbon nanotubes, fullerene, carbon quantum dots etc.) are also used to make photocatalysts to reduce pollutants. For example, Pradhan et al. prepared α-Fe_2O_3 nanorods/ reduced

105 graphene oxide composites through a hydrothermal pathway, and studied its
106 degradation properties for phenol [49]. Pawar et al. studied the stable plasma
107 photocatalysts of gold nanoparticles, g-C_3N_4 and CNTs, researched the
108 photodegradation of organic compounds. In addition, hydrogen was produced by
109 decomposing water by photoelectrochemical reaction [50]. Fullerene C_{60} is soluble
110 in conventional solvents at room temperature, and has strong antioxidant capacity
111 and stability. C_{60} has high electronegativity to accept more electrons, and has rich
112 redox properties. However, fullerene C_{60} has low solubility in water, easy
113 agglomeration, low dispersibility, and high use cost. CNTs have high electrical
114 conductivity and large specific surface area, and are chemically inert and thermally
115 stable. Reduce material agglomeration, increase dispersibility, adsorption capacity
116 and active sites. But CNTs have poor biocompatibility and cause certain harm to the
117 environment. Size has a large effect on its performance and is difficult to control [51,
118 52]. Graphene has a large specific surface area and contact area, excellent adsorption
119 capacity and mechanical properties, and high strength. It is very conductive, has
120 high charge mobility at room temperature, and is not affected by temperature. It can
121 be produced at low cost, on a large scale, and can be used as a good catalyst support.
122 However, due to the limitations of the preparation method, the intrinsic defects in
123 the graphene structure affect its properties, including thermodynamic properties,
124 electrical conductivity, etc [53-55]. Graphdiyne has abundant carbon chemical bonds,
125 large conjugated system, wide interplanar spacing, excellent chemical stability,

semiconductor properties, high order and low defects. However, the controllable preparation technology is not very mature, the cost of materials is high, and the practical application needs further research [56, 57].

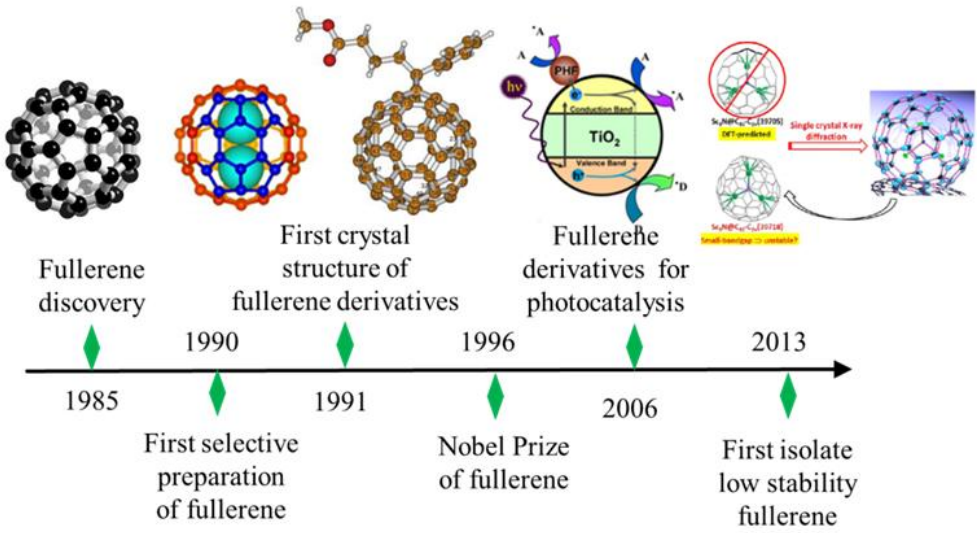

Fig.1. Illustration of the development of fullerenes and their derivatives.

In most fullerene-based photocatalytic nanomaterials, since fullerenes (especially C_{60}) have a narrow band gap (approximately 1.6-1.9ev) and a unique three-dimensional structure, which ensures the minimal changes of structure and salvation associated with electron transfer, and fullerenes (especially for C_{60}) are considered to be excellent electron acceptor and transporter. These can result in rapid charge separation on the catalyst, while at the same time producing a relatively slow recombination of electrons and holes [58]. The light-induced electron transfer process of fullerene C_{60} nanomaterials has caused great concern [59-61]. Fullerenes have great applications in many fields such as photovoltaics and photocatalysis because of their unique electronic properties and structure [62-65].

Although fullerenes have many advantages, the dispersion and solubility of fullerenes in solution are not very good. Therefore, the modification of fullerenes to obtain their derivatives for photocatalytic reaction received great attention. For example, Bai et al. modified the fullerene with a hydroxyl group to obtain a polyhydroxy fullerene, and then combined with titanium dioxide to prepare a photocatalyst for removing the organic dye [66]. Djordjevic et al. prepared a composite catalyst of polyhydroxy fullerene and titanium dioxide, and studied its degradation efficiency on herbicide mesotrione [67]. In order to obtain higher reactivity, organic catalysts prepared by composite of fullerenes and organic compounds had also made some progress [68-71].

More and more researches have been carried out on the rapid development of the preparation technology of fullerenes and their derivatives. In recent years, research on composite nano-photocatalytic materials based on fullerenes is rapidly developing, and many researchers have achieved encouraging results. For example, in the removal of organic pollutants, photocatalytic hydrogen production, photovoltaic cells, photocatalytic organic synthesis, sterilization and other aspects have achieved excellent results [68, 72-74]. Although there are many applications of fullerenes and their derivatives in photocatalysis, there is no review article that systematically studies this field. Therefore, the current comprehensive review of this specific area has important practical significance. In this paper, we outline the latest developments in photocatalytic applications based on fullerenes. The factors

affecting material effectiveness and synthesis strategies, action mechanism and applications of composites based on C_{60} and its derivatives in photoelectrochemistry and photocatalysis are elaborated, respectively. Ultimately, some challenges and promotions of fullerenes in the field of photocatalysis are discussed. This article will supply a scientific basis for the full application of fullerene C_{60} and its derivatives in photoelectrochemistry and photocatalysis, in order to achieve large-scale applications in the near future. A simple development of fullerenes and their derivatives is illustrated in Figure 1.

2. Action mechanisms of photocatalysts modified by fullerene C_{60} and its derivatives

2.1 Basic structure of fullerene C_{60}

Regarding fullerenes, its existence was forecast in 1970 [75]. The discovery of C_{60} is derived from the spectral study of the carbon atom family in the interstellar space, and the cage structure of the C_{60} molecule is proposed based on the C_{60}-based carbon atomic mass spectrogram obtained in the laboratory. 60 carbon atoms make up 20 six-membered rings and 12 five-membered rings, composed of 60 vertices, all carbon atoms are equivalent [76, 77]. Fullerene C_{60} is spherical, and the σ bond of C_{60} is different from SP^2 hybrid σ bond in graphite and diamond SP^3 hybrid bond. In spherical C_{60}, the angle between two σ bonds is 106°, and the angle between σ bond

and π bond is 101.64 °, the radius of the molecule is about 0.335 nm. C_{60} molecules are in a thermodynamic disordered state in solids and are anisotropic [78].

Theoretical calculations show that there are two kinds of C-C bonds in the C_{60} molecule: single bond and double bond, the pentagonal ring has only a single bond, and in the hexagonal ring, the single bond and the double bond are alternately arranged, so the common edge of the hexagonal ring and the pentagon ring is a single bond, and the common edge of the two hexagon rings is a double bond. The average bond length of the single bond is 0.145 nm, and the double bond is 0.141 nm [79]. The interaction force between the C_{60} molecules in the C_{60} solid is van der waals force [80], and the cohesive energy of each C_{60} molecule is 1.6 eV. At very high temperatures, although the vibrational vibration of carbon atoms is large, the cage structure of C_{60} molecules remains unchanged, indicating excellent high temperature stability[81]. According to the periodic bond chain theory, the possible crystal surface can be predicted. C_{60} crystals have a face-centered cubic (FCC) structure at room temperature. In general, when only the nearest neighbor interaction is considered for the FCC lattice, just two crystal planes {111} and {200} may exist. When the subnearest neighbor interaction is taken into account, then {220} crystal face may appear. If the third neighbor interaction is further considered, the {420}, {311}, {531} crystal faces may appear. Since the nearest neighbor interaction accounts for about 96% of the C_{60} lattice energy, other interactions are negligible. In fact, since the growth rate of the {220} crystal plane is much larger than the growth

rate of the {111} and {200} crystal planes, the {220} crystal plane will disappear during the growth process, and it is impossible to appear as a stable interface on the outside of crystal.When observing the surface morphology of C_{60} single crystals, no interface other than {111} and {200} crystal faces has been found [82]. Most C_{60} crystal surfaces are very smooth in microscopic size, but on the surface of some crystals, there are still microscopic steps on it. Fullerene C_{60} has such a suitable three-dimensional structure, and has a large number of applications in real life (Fig.2), for example, in addition to the latest research progresses in the field of photoelectrocatalysis [83-87], fullerene C_{60} and their derivatives have also been studied in photodynamic therapy [88, 89], especially in drug delivery and anti-tumor bacteria [90, 91]. Because fullerenes are biologically stable and can be linked to many drugs via covalent bonds, they have the potential to produce sustained release systems. This drug delivery strategy greatly increases the use of fullerenes and their derivatives. Fullerene C_{60} and their derivatives are also rapidly developing in the field of solar cells [92-96]. It is mainly used as acceptor material and cathode modification layer of organic polymer solar cells, and the electron transport layer of the perovskite solar cell and its modified layer. For example, Arivazhagan et al [94]. found that the C_{60} as an electron transport layer of solar cells can reduce physical defects, enhance electron extraction, and improve photovoltaic performance under appropriate thickness control. Fu et al [97]. used amphiphilic fullerenes to improve the quality of perovskite films

and the stability of perovskite solar cells. Moreover, due to the advantages of light weight, large area, and flexibility, the use of C_{60} derivatives and conjugated polymers to prepare thin film photosensors has received increasing attention [98-101]. In this article we mainly discuss its application progress in the field of photocatalysis, which we will discuss in detail in the section 4.

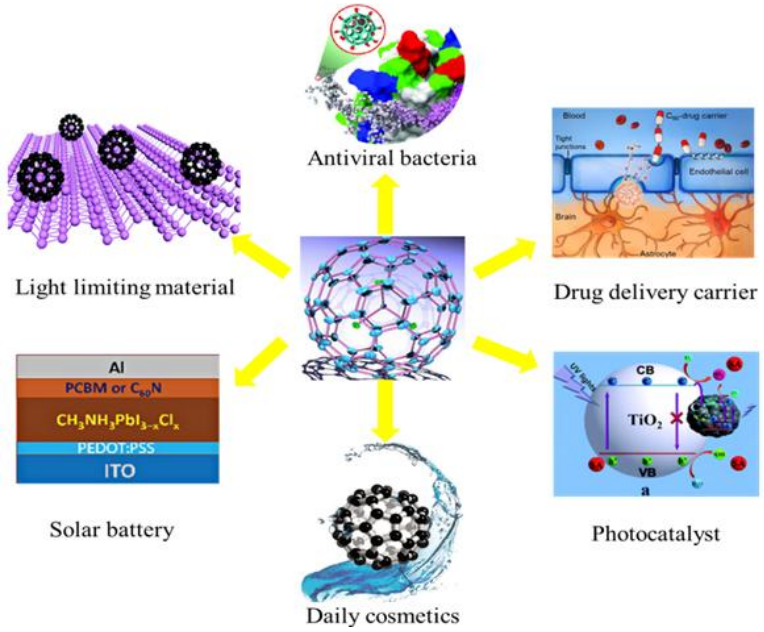

Fig.2. Main applications of Fullerene C_{60} and its derivatives.

2.2 Fullerene C_{60} derivatives

A series of derivatives of fullerene C_{60} were synthesized by modification inside or outside of fullerene C_{60}. These derivatives are used in a variety of ways to demonstrate extraordinary potential application value. In order to better understand and develop fullerenes, we need to have a comprehensive understanding of its types. The derivatives of fullerene C_{60} are mainly divided into two categories. One is

chemically modified derivatives inside fullerene cages, another is chemically modified derivatives outside fullerene cages [102-104].

In-cage modification of fullerenes refers to a special type of molecule formed by embedding metal, non-metal atoms and metal-containing clusters and molecules into a fullerene cage, namely inlaid fullerenes. The inlaid fullerene not only has fullerene properties but also has excellent properties of embedded groups, thereby expanding the application range of fullerenes. The fullerene derivatives can be classified into embedded single metal fullerenes, embedded polymetallic fullerenes, embedded non-metal fullerenes, and embedded molecular cluster fullerenes according to the embedded groups therein [102]. This second type of derivative is chemically modified outside the carbon cage. By chemical modification outside the cage, the solubility, photoelectric properties and biochemical properties of the molecules can be regulated, at the same time, functional and specific groups can also be introduced to obtain special-structure and special-purpose fullerene derivatives [105].

In this paper, we mainly introduce the derivatives obtained by chemical modification out of the fullerene C_{60} carbon cage according to the existing literatures. They are C_{60} derivatives containing hydroxyl groups, amino groups and metals [106-110]. Due to the difference of the modifying groups, different derivatives have different methods in forming composite photocatalysts. More specifically, when a hydroxyl-modified fullerene derivative forms a composite photocatalyst, it is

generally ultrasonically dispersed to obtain a better dispersion, and then the pH is adjusted to an optimum condition, finally, the hydroxyfullerene is adsorbed onto the semiconductor material by electrostatic adsorption [66, 107]. In the preparation of the composite photocatalyst with amino fullerene, a water-soluble condensation reagent is added, and the pH is adjusted to obtain an optimum coupling condition to ensure a stable linkage between the composite materials [111, 112]. As for the metal-containing fullerene derivatives [110, 113], a sol-gel method is usually used in the preparation of the composite photocatalysts. In order to ensure the stability of the metal groups, the sol is generally mixed and refluxed at a low temperature to form a gel after stirring, and then heated at different temperatures to form a composite photocatalyst.

2.3 Exclusive properties of fullerene C_{60}

As we mentioned before, carbon nanomaterials have very rich physical and chemical properties. Structure and hybrid orbit of several allotropes of carbon as shown in Figure 3. As an important member of the carbon nanomaterial family, fullerenes naturally have many properties. Fullerene C_{60} is one of the most studied materials at this stage. C_{60} has many physical and chemical properties such as non-toxicity, solubility, superconductivity, limiting effects, and so on. Obviously, its exclusive properties in photocatalytic reactions have attracted our attention. These exclusive properties of fullerene C_{60} in photocatalytic reactions are mainly

manifested in three aspects. The first is its unique morphological structural properties, followed by its optical physical properties after being excited by light, and finally the properties of derivatives derived from other functional groups.

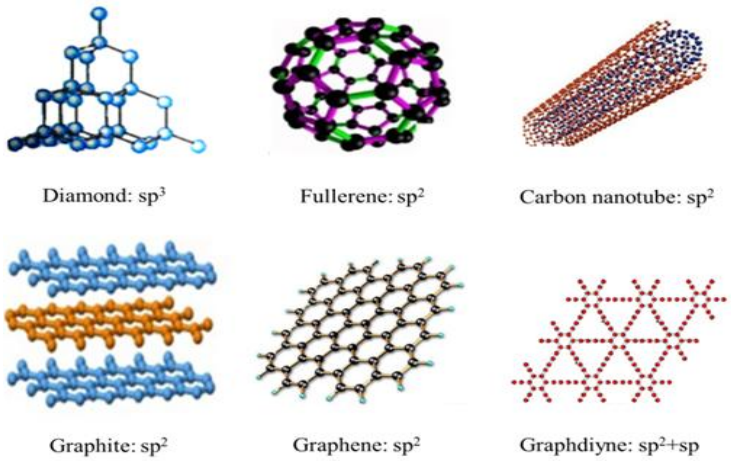

Fig.3. Structure and hybrid orbit of several allotropes of carbon.

The morphological structure of fullerenes affects its photocatalytic properties because it has a three-dimensional symmetry structure and has many micropores inside. This excellent structural feature gives C_{60} molecules high quantum efficiency in photocatalytic reactions，and it has good physical and chemical stability, can ensure the stable existence of C_{60} in the composite materials, and plays a good role in the photocatalysis process [59, 105, 114, 115].

The second point is the optical properties that are unique to it after excitation by light, including electron and energy transfer processes. Based on the semiconductor band theory, the mechanism of photocatalyst performance enhancement after fullerenes combined with semiconductor can be analyzed. Literature studies have shown that the full band gap of solid fullerenes is 1.6-1.9 eV

[86, 116]. From a photochemical point of view, fullerenes are very attractive carbon nanomolecules because they can absorb the entire visible and ultraviolet spectrum and the photocatalytic reaction is well applied in the visible range.

The third is that functional fullerene is an effective way to adjust its electronic properties. The fullerene derivatives are products of fullerene chemically functionalized and some of them have excellent properties in this field. For example, polyhydroxy fullerenes are derivatives formed by fullerene undergoing hydroxylation. After chemical modification, its properties have changed dramatically, including not only water soluble, biodegradable, but also resistant to oxidation [66, 87]. Polyhydroxy fullerene acts as an electron scavenger to promote efficient separation of photogenerated electrons and holes, as the same time, it can cause more hydroxyl radical generation. Photocatalytic generation of hydroxyl radicals increases and promotes photocatalytic efficiency. Since the chemical moiety containing a great amout of electrons has high sensitivity to singlet oxidation, chemically functionalized fullerenes achieve effective degradation of organic pollutants (eg, chlorophenols and pharmaceuticals) [112]. In addition, functionalized fullerenes are promising precursors for the efficient synthesis of fullerene nanomaterials. Derivatives that can be processed in solution allow chemical modification of fullerenes with various molecules or nanoparticles by functionalization [109]. Moreover, fullerenes can also help nanomaterials grow and become dispersible materials.

2.4 Photocatalytic enhancement mechanism of fullerene C_{60} and its derivatives

In the previous chapter, we briefly introduced the basic structure and excellent properties of fullerenes. According to our theoretical knowledge, we know that fullerenes and their derivatives must have a wide range of functions in the field of photocatalysis. These catalysts based on fullerenes and their derivatives have excellent effects in these applications. In the forthcoming content, the mechanisms of fullerenes and their derivatives in composite catalysts will be emphasized. Their photocatalytic mechanisms are analyzed by their roles in photocatalytic reactions. It includes three different functions i.e., electron acceptor, energy-transfer mediator, electron donor, and plays different roles under different conditions. When the semiconductor material is excited by light, photogenerated electrons are generated on the valence band, and the electrons are then transferred to fullerenes, where the fullerenes act as electron acceptors and transporters. Since fullerene has a small band gap and itself has a visible light response, it can directly as an energy transfer-mediator to produce $^1O_2$ for reaction. However, there is also a case where fullerenes act as electron donors, which are excited by light to transfer electrons to the semiconductor material, increase the carrier transport rate, and enhance photocatalytic activity [117-120]. Moreover, as far as we know, they can serve as electron-transfer mediator, passing electrons to other substances while accepting electrons.

Fullerene and its derivatives have a certain influence on the composite material in addition to the roles in electron transfer. According to the researches of many literatures, we know that fullerenes have the following effects on semiconductor materials: (1) regulate the growth of semiconductor crystals, (2) reduce inactivation of semiconductor materials, (3) adjust the band gap structure of the semiconductor. Fullerenes enhance the activity of the entire photocatalytic reaction by acting in the electron and energy transport and material preparation processes.

2.4.1 Electron and energy transfer in photocatalysis

2.4.1.1 Fullerene as an electron acceptor

Fullerene (C_{60}) is known to be one of several allotropes of carbon, differing from others in that it has unique electronic properties. The closed shell composed of C_{60} contains 60 π electrons composed of 30 bonding molecular orbitals, which is beneficial to reduce effective electron transfer. Fullerenes are electron acceptors in composite catalysts. On the one hand, they can effectively separate light-induced charges and generate a large amount of electrons. On the other hand, the re-contact of photogenerated electrons and holes is also suppressed [121, 122].

When the fullerene material is irradiated with light, C_{60} is excited from the ground state to a short singlet excited state in a short time (about 1.2 ns), and then rapidly from a single state to a lower triplet state ($^3C_{60}$*) through intersystem crossing (ISC) process(Fig. 4A). The triplet C_{60} has a very long lifetime (> 40 μs).

The visible light-excited C_{60} becomes a good electron acceptor, and its ability to accept electrons is greatly enhanced, and it can accept up to 6 electrons. This is the most important for enhancing the reactivity. Triplet C_{60} has stronger electron accepting ability than ground state C_{60}, and a C_{60} radical anion ($^3C_{60}^-$) can be obtained by the reaction. Excited state $^3C_{60}$* will accept electrons from semiconductor materials, namely electron donors (ED), then the $^3C_{60}$* is reduced to $^1C_{60}^{\cdot-}$ (Fig. 4B). In turn, a series of reactions between the reactants at the interface and the radical species are generated. Further, the nano fullerene material can produce electrons and holes under the excitation of light. Therefore, fullerene carbon nanomaterials can effectively promote rapid photoinduced charge separation, strengthen the production of photogenerated electrons and holes, and achieve the purpose of enhancing photodegradation performance [123]. Fullerenes have been combined with various wide band gap semiconductor photocatalysts as novel composite photocatalysts for photocatalytic reactions, such as TiO_2 [121, 124-126], ZnO [127], BiOCl [128].

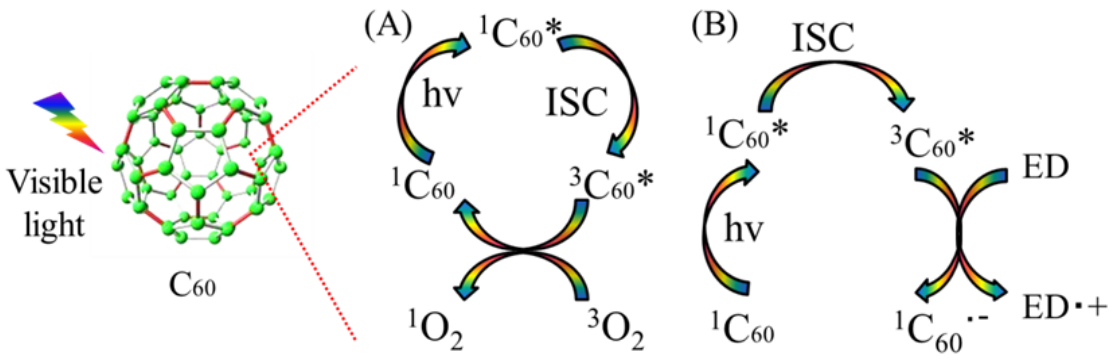

Fig. 4. Photochemical pathways of C_{60} after light excitation: (A) energy-transfer and (B)

electron-transfer [129]. Copyright 2010 Elsevier.

Yu et al. [121] prepared a nanocomposite catalyst of fullerene and titanium dioxide by simple hydrothermal crystallization method for photocatalytic degradation of vapor phase acetone. According to the experimental results, it was concluded that C_{60} played an electron acceptor and a transporter in the photocatalytic process to help improve electron mobility. In this system, the conduction band potential of titanium dioxide was more negative [118]. Therefore, electrons in the composite material could be smoothly transferred from titanium dioxide nanoparticles to fullerenes. When the photocatalyst was active, the valence electron (e^-) of the anatase type titanium oxide was excited to the conduction band of the catalyst, and holes were generated in the valence band. Usually, as a result of the rapid recombination of these charges, just a relatively small portion of the electrons and holes played a role in the whole process. However, if the titanium dioxide nanoparticles are chemically bonded to the fullerene molecules, these electron transfer tendencies change dramatically and they begin to shift to C_{60}.

In addition, researchers have learned through experiments that this effect of fullerenes is affected by many conditions, including fullerene content, interactions between fullerenes and semiconductor, and contact areas. In this role, the controllable photocatalytic activity of fullerene and semiconductor nanocomposites has been extensively studied by changing the fullerene content. For example, Fu's research group [127] studied the photocatalytic properties of C_{60}/ZnO photocatalysts.

The composite catalyst was studied for its catalytic performance by using the degradation efficiency of acid red 18 as an index. With the increase of C_{60} content, the efficiency of composites degrading pollutants was continuously improved, and the degradation effect reached the optimum value at 1.5% C_{60}. This might be due to the fact that too much C_{60} became a complex center of photoelectron-hole pairs. They believed that the enhanced performance was because of the role of fullerenes in electron acceptors and transporters in composites. Ma et al. [128] prepared a C_{60}/BiOCl composite catalyst by in-situ preparation. Degrading the organic dyes rhodamine and phenol under simulated sunlight, 1.0% C_{60}/BiOCl had the vintage degradation rate constant. Fullerene C_{60} accepted electrons and rapidly transferred to the catalyst to react rapidly with contaminants, which caused a valid strengthen in degradation efficiency. The successful transfer of electrons to the non-localized π-bond structure of fullerenes allowed the charge of the composite catalyst to be continuously separated and continuously transferred, thus the reaction proceeds continuously.

It is known to all that, invisible light energy in the ultraviolet region accounts for 4% of total sunlight energy, and most of the sunlight energy is occupied by visible light. Therefore, by introducing fullerenes as electron acceptors and transporters, the synthesis of novel composite photocatalysts is gradually being noticed. Among photocatalysts that function in the visible range, carbon nitride, with band gap as 2.7 eV, is a potential material that can achieve high reactivity.

413 Unfortunately, the photocatalytic efficiency of g-C_3N_4 is restricted because of the
414 rapid recombination of electrons and holes. Bai et al. [72] used a simple
415 conventional heat treatment process to synthesize C_{60}/g-C_3N_4 composites. After C_{60}
416 modification, the photocatalytic activity of graphite phase carbonitride for degrading
417 pollutant MB and phenol was greatly improved. Studies had shown that under
418 experimental lighting conditions, the composites had good electron conductivity,
419 which made these photoelectrons on g-C_3N_4 CB easy to transfer to C_{60} particles. C_{60}
420 quickly accepted electrons and transfers it to the surface of C_{60} to adsorb oxygen to
421 form superoxide radicals, which in turn oxidized pollutants. The addition of
422 fullerenes could effectively slow down the contact rate of electrons and holes,
423 improved the survival time of photogenerated electrons, and enhanced the
424 degradation efficiency. Chai et al. [130] prepared a fullerene-modified C_3N_4
425 (C_{60}/C_3N_4) composite by adsorption method, which had sensational reactivity.
426 Experiment to degrade organic pollutant rhodamine as a target pollutant, and the
427 excellent degradative energy was synergistic between C_{60} and C_3N_4. And this
428 synergy facilitated electron transfer. Since the content of fullerene C_{60} in the
429 composite catalyst had a great influence on its electron acceptor and transfer body,
430 the research team found that when the mass fraction of C_{60} was 1%, the catalyst
431 exhibited the largest electron transport efficiency and obtained the maximum
432 photocatalytic efficiency. Mechanism of action of fullerenes in electron transport is
433 illustrated in Figure 5.

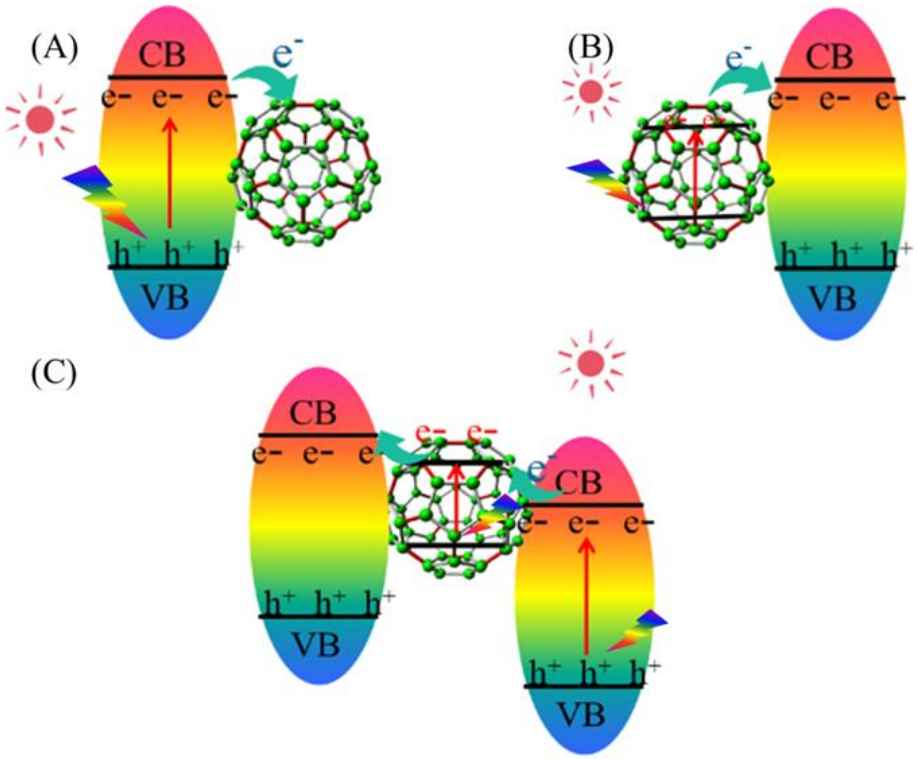

Fig. 5. Mechanism of action of fullerenes in electron transport: (A) fullerene as an electron acceptor, (B) fullerene as an electron donor, (C) fullerene as electron acceptor and donor.

2.4.1.2 Fullerene as energy-transfer mediator

Through the above section, we know that fullerene C_{60} and its derivatives can act as electron acceptors in composite catalysts, the electrons are quickly accepted and moved to the catalyst, thereby greatly delaying the recombination rate, and then achieving the purpose of improving photocatalytic efficiency. Moreover, fullerene C_{60} and its derivatives can be directly used as energy-transfer mediator due to their unique optical properties. The mechanism of fullerene C_{60} as an energy transfer mediator is mainly related to the description of the photochemical path of C_{60} under

light excitation. When light is irradiated to the fullerene C_{60} in the ground state, the fullerene C_{60} absorbs energy, and the singlet state C_{60} changes to the singlet excited state C_{60}. In order to reach a more stable state, it then undergoes intersystem crossing (ISC) to a longer-lived triplet excited state ($^3C_{60}$*). The ground state oxygen molecule ($^3O_2$) is an effective quencher for the triplet excited state fullerene C_{60}. When triplet fullerene C_{60} contacts the ground state oxygen molecule, it transfers its own energy to the ground state oxygen molecule, and the ground state oxygen molecule is excited, then a singlet oxygen molecule ($^1O_2$) is formed (Type II energy transfer process) [131]. The singlet oxygen molecule has a strong oxidizing ability and can participate in the degradation of pollutants and the catalytic synthesis of organic matter. Due to the input of light energy in this whole process, the energy transfer process was completed with the help of fullerene C_{60} as an energy transfer mediator[129, 132-134].

C_{60} and its derivatives enhance the production of $^1O_2$ with the aid of visible light (or sunlight) and utilize the oxidizing power of $^1O_2$ for pollutant degradation and microbial inactivation. Lee et al. [109] used C_{60} aminofullerene to covalently bond with surface-functionalized silica gel to prepare a photocatalyst. The experimental results showed that C_{60} amino fullerene was uniformly dispersed on silica gel. Under visible light irradiation, compared with C_{60} amino fullerene aqueous solution, amino C_{60}/silica photocatalyst had better kinetic enhancement for degradation of some drug contaminants and inactivation of MS-2 phage. On the one

hand, since the amino fullerene had a suitable band gap, it as energy-transfer mediator to absorb light energy, then it could be excited by visible light to generate $^1O_2$, and directly to remove contaminants. On the other hand, amino C_{60}/silica enhanced photoreactivity because it prevented the aggregation of fullerenes on the silica, increased the reaction area to some extent, and finally achieved the purpose of delaying the electron self-quenching mechanism. Panagiotou et al. [129] used a dipping method to disperse fullerenes on the surface of silica, and the photocatalyst prepared thereby had high dispersibility and stability. The amount of C_{60} was 1-4% (w/w) range. Fullerene C_{60} was directly served as energy-transfer mediator to explore the photocatalytic activity of the catalyst by oxidative decomposition of the compound 2-methyl-2-heptene. After the fullerene was excited by light, absorbed energy and produced singlet oxygen to participate in the redox reaction, thereby effectively promoted photocatalytic efficiency.

2.4.1.3 Fullerene as an electron donor

As mentioned above, fullerenes have been widely accepted as accepting photogenerated electrons from photoexcited semiconductors. However, some experimental and theoretical studies have also observed the transfer of photoexcited electrons from fullerenes to semiconductors. It is due to the electron transfer process of fullerene under light irradiation that fullerene act as photosensitizer to provide electrons to semiconductor materials. Kamat et al. [135] reported that they used

different testing techniques to study the charge transfer process between semiconductor nanomaterials and fullerene materials, and found that fullerene C_{60} was photoexcited and photogenerated electrons transfer from C_{60} to the surface of TiO_2. Later, Makarov et al. [136] experimentally measured the change in conductivity of the fullerene layer. The results showed that the TiO_2-C_{60} multilayer structure is photosensitive.

In summarizing the work of the predecessors, the researchers fully explained the photosensitivity effect of fullerenes. The general processes of this action are as follows: the electrons in the highest occupied orbit of fullerenes are first excited by light to the lowest unoccupied orbit of fullerenes, and then the photogenerated electrons in the fullerene are transferred and they are impregnated into the CB of the semiconductor material. Finally, the reduction reaction is completed on the surface of the semiconductor to exert its function as a electron donor.

Generally, fullerenes have a special morphological structure and a strong electronic structure. When it is compounded with other catalysts and attached to its surface, it acts as a electron donor. Therefore, it participates in the photochemical process of the photocatalyst surface and sensitizes the photocatalyst. Recently, Grandcolas et al. [116] had explored a simple preparation of C_{60} sensitized TiNTs composites used an organic solvent impregnation process, the effect of explored fullerene concentration on the preparation of TiNT was analyzed. The adhesion of fullerene substances to TiNTs was evaluated. They found that C_{60} sensitization

effectively enhanced the removal of gaseous organic pollutants. The removal of the contaminant isopropanol under visible light showed higher efficiency. Meng et al. [113] synthesized a fullerene and titanium dioxide composite nanophotocatalyst, and the fullerene used in the experiment was treated with rare earth oxide, and the composite catalyst exhibited a single anatase phase. The results revealed that the yttrium-fullerene/TiO_2 composite had good photodegradation activity of the organic dye methylene blue. Fullerene was used as a electron donor in a composite catalyst formed after the combination of fullerenes and TiO_2 nanomaterials, and when it was excited by visible light, the photogenerated electrons were transferred by the photosensitizer and reacted to the surface of the semiconductor material. It was owing to the coordinate reaction of TiO_2, fullerene and yttrium that yttrium-fullerene/TiO_2 had good light absorption. On account of its good light absorption properties, the composite catalyst had good photocatalytic activity.

In addition, the research team also studied the preparation of platinum-treated fullerene and titanium dioxide composite nanocomposites by the same method [137]. Fullerenes were distributed on the titanium dioxide material and reached a good dispersion state, and the metal also had a high degree of dispersion on fullerene and titanium dioxide, therefore, the composite catalyst had an excellent catalytic effect on the removal of MO. Pt could delay the recombination of charge pairs and captured electrons. Therefore, Pt-TiO_2 had good adsorption properties and could improve the catalytic activity of the material.

When fullerenes are combined with semiconductor materials, fullerene is acted as a electron donor after being excited by light, realize the transport of electrons to semiconductor materials and also enhances the BET surface area effect of fullerenes due to its photosensitivity. This effect of fullerene nanomaterials has not been fully explored in the treatment of pollutants, but also in photocatalytic water cracking. For example, Song et al. [138] successfully prepared C_{60} and $Cr_{2-x}Fe_xO_3$ composite nanostructured photocatalysts by simple absorption process and used it for photocatalytic H_2 production. The results showed that photoelectrons achieved high mobility at the C_{60} and $Cr_{2-x}Fe_xO_3$ interfaces, this was owing to the strong interaction of this composite catalyst with the internal d of the conjugated three-dimensional π-system. After the composite photocatalyst was synthesized by C_{60}, the light absorption intensity of the composite catalyst containing 3% C_{60} was the largest, which was mainly because of the effect of C_{60} as a electon donor to provide electrons on the composite catalyst.

According to the previous analysis, we have basically understood that C_{60} plays an important role in the electron transfer system, that is, the electron acceptor and the electron donor. As far as we know, there are mainly two conditions affect the electron transfer process, one is light and the other is the band structure of semiconductor materials [72, 137, 139-141]. When C_{60} is combineed with a wide band gap semiconductor material, and irradiated with visible light, the part of semiconductor cannot be excited, and C_{60} can be excited by visible light to generate

photo-generated electrons. The level of the conductive band of a semiconductor material is lower than the reduction potential of C_{60}, so photo-generated electrons can be easily transferred from the conductive band of C_{60} to the molecules where C_{60} interacts with the semiconductor material. In this electron transfer process, C_{60} acts as an electron donor to provide electrons to participate in the reaction. In some ternary photocatalysts with proper energy level relationship, C_{60} can be excited by visible light to transfer electrons to the conduction band of a narrow band gap material, and also participate in the reaction as an electron donor.

When C_{60} is compounded with a semiconductor material that responds to visible light, it reacts under visible light to generate photo-generated electrons that are transferred to C_{60}. These electrons are accepted by the C_{60} electron acceptor. From another perspective, when semiconductor material is UV-responsive, the electrons excited by UV light are transferred to C_{60}, and the electrons are accepted by fullerene. In both cases, C_{60} acts as an electron acceptor to participate in photocatalytic reactions.

2.4.1.4 Fullerene as electron acceptor and donor

Through the analysis of the above subsections, we know that fullerenes and their derivatives play an important role in the electron and energy transfer process of photocatalytic reactions. As an electron acceptor, energy transfer-mediator, electron donor. It is precisely because of the excellent effects of fullerenes and their

derivatives that the efficiency of photocatalytic reactions is significantly improved. According to our research, we found that there is another path for electronic transfer. That is, fullerene is used as an electron acceptor in the complex system, and at the same time, it can be excited by light to generate photogenerated electrons and holes, and the electrons are transferred to another material to generate radicals or a reduction reaction. Meng et al. [142] prepared a composite photocatalyst of WO_3 modified fullerene/TiO_2. Due to the narrow band gap of WO_3, photogenerated electrons can be generated under illumination and transferred to the fullerene surface. At this time, fullerenes act as electron acceptor, and at the same time, fullerenes are photoexcited for electron transfer, and electron flow to TiO_2 due to the suitable conduction band of the three species.

2.4.2 Effect of fullerene on composite materials

The photocatalytic performance of a composite material is not only related to the chemical properties of the material, but also the morphology and structure are also important influencing factors. In addition to electron transport and energy transfer, fullerenes and their derivatives have a great influence on composite materials in photocatalytic reactions. Specifically, it includes three aspects, regulating the growth mode of the crystal to obtain a better morphology structure, reducing the deactivation rate of the material in the reaction to ensure the stability of the catalyst, and adjusting the band gap of the composite material to obtain a higher

light absorption range. The specific role of fullerenes in composites will be discussed in detail in the following sections.

2.4.2.1 Regulation of crystal growth

Fullerene C_{60} plays a role similar to templating and dispersing agents in regulating the crystal growth of composites [128]. When fullerene C_{60} is added in the synthesis of composite materials, the solid-liquid interface energy of different growth crystal planes will be changed, and the growth rate of each crystal plane will be adjusted. Different crystal planes have different growth rates, when C_{60} is added, the growth of a certain crystal plane is inhibited, and finally the growth mode and morphological characteristics of the semiconductor material crystal are changed [72].

When synthesizing composite materials, fullerene C_{60} can regulate the crystal structure of semiconductor materials in order to obtain better morphology structure. It is well known that having good morphology is likely to have high photocatalytic efficiency in photocatalytic reactions. Ma et al. [128] prepared C_{60}/BiOCl composites by in-situ hydrothermal method. The experimental results show that the addition of C_{60} slightly increases the surface area of the raw materials, and thus more surface active sites can be obtained. More importantly, the addition of C_{60} effectively inhibited the growth of BiOCl {001} crystal plane. It was found that the vibration of Bi-Cl in the composite material was blue-shifted, indicating that the two

materials were not simply physically mixed. The morphology of the composite is significantly different from that of a single BiOCl, C_{60} plays a regulatory role in the growth of BiOCl microsphere. Bai et al. [72] found that in the C_{60}/g-C_3N_4 composite, the TEM image can be used to analyze the composite material with higher crystallinity and better crystal morphology. This also showed that fullerenes had a certain effect on the crystal structure of carbon nitride. The regulation of the crystal structure of the composite by fullerene allows the composite to have good morphology and high crystallinity, thereby effectively increasing the reactivity of the composite photocatalyst.

2.4.2.2 Reduce material deactivation rate

Photocatalytic technology has many applications in the fields of environmental remediation and clean energy generation. On the one hand, materials selected as photocatalysts must first have good photocatalytic activity to ensure the high efficiency of photocatalytic reactions. On the other hand, from the perspective of resource conservation and practical application, the prepared catalyst should have good stability and environmental tolerance. Therefore, it is important to ensure the activity of the catalyst in the photocatalytic reaction and prevent the deactivation of the photocatalyst.

The general mechanisms of the inhibition of fullerene C_{60} and its derivatives on the deactivation rate of composite materials are mainly manifested in two aspects.

The semiconductor in the composite material may have polycrystalline and amorphous structures in the crystal structure during the photocatalytic reaction, causing the loss of some elements, which in turn leads to a decrease in the driving force of the lattice and the activity of the material. After hybridization with fullerene C_{60}, a dense monomolecular layer is formed on the surface of the semiconductor material, fullerene C_{60} is similar to support material and protects material from deactivation [143]. There is a close interaction between them, which protects the crystal lattice of the composite material from being changed. Some bonds of semiconductor materials exist in an unsaturated state (such as oxygen atom bonds). After the reaction, the crystal structure of the semiconductor material collapses, forming a series of defect sites, and fullerene C_{60} anchoring in these vacancies enhances the binding ability with semiconductors, eventually suppresses material deactivation [127, 144].

In composite photocatalysts modified with fullerenes and their derivatives, for some unstable semiconductor materials, the absence of elements or the increase of molecular surface defect sites may occur during the reaction. These materials are then gradually lost as the reaction progresses, and the activity is greatly reduced. When the fullerene is added, the photochemical corrosion process of the semiconductor can be effectively suppressed, thereby ensuring the photocatalytic efficiency of the composite photocatalyst. For example, Du et al. [144] prepared a $C_{60}/Bi_2TiO_4F_2$ composite photocatalyst to achieve good results in depolymerization

651 of lignin. It was found that when a single $Bi_2TiO_4F_2$ was reacted as a photocatalyst,
652 the material deactivation rate was high. As the reaction progressed, the loss of Bi in
653 the material became more and more serious. It was observed that the edge of the
654 crystal lattice was blurred, and a polycrystalline or amorphous structure appeared,
655 which caused the lattice driving force to be weakened, thereby reduced the
656 photocatalytic ability. In the $C_{60}/Bi_2TiO_4F_2$ composite, the activity of the material
657 was obviously improved, which was attributed to the close interaction of C_{60} and
658 $Bi_2TiO_4F_2$, which reduced the loss of Bi element, ensured the stability of the
659 material and improved the photocatalytic efficiency. Fu et al. [127] found that ZnO
660 as a photocatalyst had strong photocorrosion due to enhanced activation of surface
661 oxygen atoms. C_{60} bonded to the surface of ZnO and formed a monolayer. After
662 introduced C_{60}, it can occupy the defect site of ZnO surface and act as the anchor
663 point of C_{60}, which reduced the activation of surface oxygen atoms and inhibited the
664 deactivation of ZnO. Ju et al. [143] found that in ZnAlTi-LDO supported C_{60}@AgCl
665 nanoparticles, because C_{60} has a non-localized conjugated structure, it is easy to
666 form a core-shell structure of C_{60}@AgCl, which in turn encapsulates AgCl and
667 inhibits photochemical corrosion.

668 **2.4.2.3 Adjust the band gap structure**

669 When fullerene C_{60} and its derivatives are compounded with semiconductor
670 materials, they will form a strong interaction with semiconductor materials. Such as

forming chemical bonds (metal-C-O bonds), hybridizing structures, or producing irreversible structural distortions (structural strains) [120, 145]. The formation of chemical bonds causes changes in the bond length and bond energy of semiconductor materials, which changes the band structure. The formation of a hybrid structure introduces impurity energy levels between semiconductor energy bands to regulate the band gap width. The adsorption of fullerene C_{60} on semiconductor materials will cause structural distortion, which will cause the conduction band and valence band of the semiconductor to move and change the band structure.

In the research of heterojunction composite photocatalysts, people have done a lot of exploration. At present, five types of heterojunction structures are mainly studied, they are conventional heterojunctions, p-n heterojunctions, direct Z-scheme heterojunctions, surface heterojunctions, and semiconductor-graphene (SC-graphene) heterojunctions. Typically, there are three types of conventional heterojunction photocatalysts, those with a straddling gap (type-I), those with a staggered gap (type-II), and those with a broken gap (type-III) [146, 147]. Ma et al. [120] found that in most cases, the general composite system showed a type-I heterojunction, which was not conducive to the efficient separation of photogenerated carriers. When the C_{60}/g-C_3N_4 complex was formed, the DOS change was small, indicating that the electron interaction between C_{60} and g-C_3N_4 was weak, so electron transfer was not a major factor. After the addition of C_{60} to g-C_3N_4, the adsorption of C_{60}

caused the structure of the g-C_3N_4 monolayer to change from plane to wrinkle and was irreversibly distorted, thereby moved the band edge to a lower position. As far as we know, semiconductors with lower valence bands have stronger photo-oxidation ability, which enhances the photocatalytic effect. This shows that fullerene C_{60} has a certain regulation effect on the band gap of semiconductor materials, and this effect has been found in many studies. Kanchanatip et al. [148] prepared a C_{60} modified metal vanadium doped TiO_2 composite catalyst C_{60}/V-TiO_2. The band gap of the catalyst before and after C_{60} modification was compared. It can be seen that the band gap of the composite material was significantly reduced, and the activation under visible light was easier than that of a single V-TiO_2.

3. Factors affecting material effectiveness and synthesis strategy

3.1 Factors affecting material effectiveness

In the previous sections we explored the role of fullerenes in photocatalytic reactions, including their roles in electron transfer and their effects on composites. We know that fullerenes have these excellent properties to improve the efficiency of photocatalytic reaction, but there are still some unfavorable factors that limit the application of fullerenes and their derivatives in photocatalysis. It is necessary to point out and propose strategies.

In addition to the many excellent properties of fullerenes, there are some

711 application limitations for fullerenes. First, we consider the water solubility of
712 fullerene C_{60} and dispersion in aqueous solution, the solubility and dispersion of
713 single fullerene and fullerene that has not been modified in aqueous solution is very
714 low. Therefore, the photocatalytic reaction efficiency of fullerenes in the aqueous
715 phase is limited. In order to enhance the solubility and dispersion of fullerenes in
716 aqueous solution, and to improve the photocatalytic activity, we summarize the
717 following treatments: (1) Mechanical dispersion-stabilization of C_{60} [149], such as
718 ultrasonic dispersion or solvent exchange methods [150]. However, these methods
719 generally only obtain metastable C_{60}, which eventually repolymerizes, possibly
720 resulting in uncontrolled modification of the C_{60} surface. (2) Synthesis of
721 water-soluble fullerene derivatives by chemical functionalization with hydrophilic
722 groups of pristine fullerene [151]. However, to the best of our knowledge, this soft
723 derivatization process maintains the tendency of these amphiphilic C_{60} derivatives to
724 repolymerize, affecting the reactivity of fullerenes. And in some cases multiple
725 functionalization can lead to changes in the unique structure of fullerenes, which has
726 a negative impact on specific performance, limiting the practical application. (3) Use
727 dispersant to help C_{60} achieve good dispersion in aqueous solution, such as
728 surfactants, block copolymers, amphiphilic polymers, micelles [152, 153]. The use
729 of surfactants is the most effective treatment and can be effectively dispersed when a
730 large amount of C_{60} is contained. And the obtained fullerene has aggregates of
731 different sizes, which may exist in the hydrophobic core of the dispersant or on the

surface of the dispersant. (4) Dispersed by a suitable carrier having a hydrophobic core. Generally used are γ-cyclodextrins, calixarenes and other macrocyclic-containing molecules [154, 155]. The supramolecular approach is the most effective way to obtain monodispersed pristine fullerenes. However, it is also common for fullerenes to aggregate in subsequent reactions and may be somewhat toxic to certain organisms. Fortunately, in recent studies [156], it had been found that a composite photocatalyst obtained by combining an organic substance such as a protein and fullerene exhibits monodispersion in an aqueous solution. The composite had no aggregate of C_{60} molecules, and can stably maintain several months even in a salt solution. The composite system did not require an additional electron donor (protein residues acted as electron donors) in the photocatalytic reaction to significantly affected the light-induced ROS process, and the protein environment strongly reduced the quenching effect of water molecules on singlet oxygen. The catalyst can effectively inhibit the aggregation of fullerenes, thereby improving the photocatalytic efficiency.

The experimental conditions in the preparation of photocatalysts based on fullerene and its derivatives also affect the properties of the composite under certain conditions. In general, the most influential is the concentration of fullerenes, and the concentration of fullerenes largely affects the crystal size of fullerenes in the composite [127]. When the amount of fullerene is insufficient, it is obviously unable to have the best reactivity, but when the fullerene is too much, large aggregates are

formed, and the crystal size in the composite material becomes large, which is disadvantageous for the transfer of light-induced electrons. It is also possible to reduce light absorption, which ultimately leads to reduced efficiency.

In addition, the pH value of the reaction solution also affects the properties of the composite material. Krishna et al. [106] found that under acidic conditions, the surface of the TiO_2 nanoparticles was positively charged, and the surface of the polyhydroxyfullerene was negatively attracted to the surface of the TiO_2. The density was increased, which in turn increased the catalytic efficiency. On the contrary, polyhydroxy fullerenes were repelled on the surface of TiO_2 under alkaline conditions, so that the adsorption density was lowered, the surface charge was not changed, and the catalytic efficiency was not high. And under suitable pH conditions, it is not necessary to synthesize chemical bonds by methods such as sol-gel to strengthen the interaction between the materials, and thus has a strong affinity.

3.2 Synthesis strategy of fullerene modified photocatalyst

In this subsection, the synthesis methods commonly used in experimental studies of catalysts of fullerene C_{60} and its derivatives are mainly introduced. The preparation method of the catalyst has great experimental significance for the fullerene-based composite materials, which not only affects the morphological structure of the materials, more importantly, but also has a serious impact on its photocatalytic efficiency. Choosing the ideal preparation method is critical to

achieving optimal photocatalytic efficiency. In all preparation methods, the easiest way is to simply mix, grind or calcine fullerenes and inorganic materials; complex methods involve multiple different processes. This article is mainly based on the successful preparation methods mentioned in the literature on photocatalysis of fullerene/semiconductor composites. By analyzing the results reported in the literature, the current composite methods are simple mixing, sol-gel method, hydrothermal method, solvothermal method and impregnation method. In addition, other preparation methods are also discussed including chemical vapor deposition, ultrasonic method and so on.

Composite photocatalysts with various micro/nano structures were prepared by changing the experimental conditions, containing synthesis methods, pH and time of action and reaction temperature, and the surface activity of the catalyst. The following sections describe in detail the relevant preparation methods of fullerene-based catalysts. The synthesis methods of fullerene-based photocatalysts were shown in Table 1.

788 Table 1.Methods for synthesizing fullerene-based photocatalysts.

Photocatalyst	Preparation method	Reactant solution	Main precursors	Processing temperature	Ref
TiO_2/C_{60}	impregnation method	1,2-dichloro-benzene	titanium isopropoxide	180 ℃	[157]
SiO_2/C_{60}	impregnation method	dichlorobenzene	silicon(IV) oxide amorphous fumed	180 ℃	[129]
C_{60}/MCM-41	impregnation method	1,2-dichlorobenzene	CTAB, TEOS, polypropylene	180 ℃	[158]
Ag_3PO_4/C_{60}	impregnation method	ethanol	$AgNO_3$,NaH_2PO_4	-40 ℃	[159]
Fe_2O_3/C_{60}	impregnation method	benzene	$FeCl_3$,m-chloroperoxybenzoic acid	60 ℃	[160]
C_{60}/MCM-41	impregnation method	cetyltrimethylammonium bromide	cetyltrimethylammonium bromide tetraethylorthosilicate polypropylene	180 ℃	[134]
C_{60}/γ-Al_2O_3	impregnation method	1,2-dichlorobenzene	γ-alumina	180 ℃ for 4h	[161]
TiO_2/C_{60}	impregnation method	ethanol, toluene	anatase TiO_2, NaOH	350 ℃	[116]

$C_{60}/SiO_2/Fe_3O_4$	impregnation method	toluene/ethanol	$Fe(NO_3)_3•9H_2O$, TPSA	60 ℃	[112]
$WO_3/TiO_2/C_{60}$	sol-gel method	benzene	MCPBA, TNB $H_{26}N_6O_{40}W_{12}•xH_2O$	heat treat 600 ℃	[142]
$Pt/TiO_2/C_{60}$	sol-gel method	benzene	MCPBA, $H_2PtC_{l6}•nH_2O$, TNB	heat treat 500 ℃ for 1h	[137]
$C_{60}/V\text{-}TiO_2$	sol-gel method	toluene	titanium(IV) isopropoxide, acetylacetone, acetone, ammonium metavanadate	180 ℃ for 4 h	[148]
$CoS_2\text{-}C_{60}/TiO_2$	sol-gel method	3-chloroperoxybenzoic acid	TCPBA , $CoCl_2$, $Na_2S_2O_3$,TNB	400 ℃	[123]
$MoO_3\text{-}TiO_2/C_{60}$	sol-gel method	iso-propanol/ethanol	CTAB ,titanium (IV) butoxide ammonium heptamolybdate	500 ℃ for 2h	[162]
$C_{60}/CNTs/g\text{-}C_3N_4$	hydrothermal method	ethanol	CNTs, $g\text{-}C_3N_4$, ethanol	180 ℃ for 3 h.	[163]

$Ag_3PO_4/Fe_3O_4/C_{60}$	hydrothermal method	toluene	NaOH ,$(NH_4)_2FeSO_4$•$6H_2O$, $NaBH_4$,Na_2HPO_4,$AgNO_3$	180 ℃ for 20 h	[58]
C_{60}/graphene/g-C_3N_4	hydrothermal method	ethanol	urea, graphene	550 ℃ for 3 h	[164]
BiOCl/C_{60}	hydrothermal method	HNO_3	$Bi(NO_3)_3$ 5H_2O, KCl ,nitric acid	180 ℃ for 24 h.	[128]
WO_3@C_{60}	hydrothermal method	benzene	m-chloroperbenzoic acid	80 ℃ for 24 h	[165]
Bi_2MoO_6/C_{60}	hydrothermal method	toluene	Na_2MoO_4, $Bi(NO_3)_3$	180 ℃ for 12 h	[166]
TiO_2/C_{60}	solvothermal method	toluene	$Ti(OC_3H_7)_4$,	80 ℃ for 12h	[167]
$Bi_2TiO_4F_2/C_{60}$	solvothermal method	toluene	$Bi(NO_3)_3$ 5H_2O,ethylene glycol, TiF4, tert-butyl alcohol	160 ℃ for 24 h	[168]
ZnO/C_{60}	solvothermal method	toluene	ZnO	80 ℃ for 10 h	[127]
$Cr_{2-x}Fe_xO_3$ /C_{60}	adsorption method	toluene	$Cr(NO_3)_3$ 9H_2O, $Fe(NO_3)_3$ 9H_2O, $C_6H_8O_7$, $C_2H_6O_2$, $C_6H_{15}NO_3$	80 ℃ for 12 h	[138]

Bi_2WO_6/C_{60}	adsorption method	toluene	Na_2WO_4, $Bi(NO_3)_3$	80 ℃ for 10 h	[169]
C_3N_4/C_{60}	adsorption method	toluene	urea	80 ℃ for 12 h	[130]
SiO_2/C_{60}	evaporation method	toluene	ascorbic acid, SiO_2	-	[141]
$CdS/TiO_2/C_{60}$	evaporation method	toluene	$Cd(NO_3)_2 \cdot 4H_2O$, Na_2S titanium tetrachloride	400 ℃ for 4 h	[139]
PTCDI-C_{60}	ultrasonication method	sulfuric acid	perylene tetracarboxylic diimide sulfuric acid	-	[170]
TiO_2/THF-nC_{60}	simple mixing method	mesotrione	CH_3CN, TiO_2 Hombikat,EDTA	-	[67]
Zn/Ti-LDH/C_{60}	co-precipitation method	toluene	HNO_3, $Zn(NO_3)_2$ $6H_2O$, Urea, $TiCl_4$, NaOH	80 ℃ for 12 h.	[171]
C_{60}/g-C_3N_4	thermal treatment	-	dicyandiamide	550 ℃ for 4 h	[72]
AgCl/C_{60}	coprecipitation method	ethylene glycol	NaCl, $AgNO_3$, ZnAlTi-LDO	60 ℃ for 12 h	[143]

$CoPc/C_{60}$	reprecipitation method	N-methyl-2-pyrrolidone	cobalt phthalocyanine methylpyrrolidone	−45 ℃ for 2 h	[70]
$g\text{-}C_3N_4/C_{60}$	mechanochemical method	-	dicyandiamide, LiOH	550 ℃ for 4 h	[172]
$ZnFe_2O_4@C_{60}$	hydrothermal and calcination methods	-	$Fe(NO_3)_3·9H_2O$, $Zn(NO_3)_2·6H_2O$	400 °C for 2 h	[173]
CdS/C_{60}	interfacial precipitation method	toluene	$CdSO_4$, Na_2S, polyvinyl pyrrolidone	-	[85]
SnO_2/C_{60}	interfacial precipitation method	toluene	tin (IV) chloride pentahydrate ammonium nitrate	180 ℃ for 12 h	[174]
$WO_3/C_{60}@Ni_3B/Ni(OH)_2$	facile photo-deposition method	triethanolamine	$NiCl_2·6H_2O$, $NaBH_4$, NaOH NaH_2PO_2	-	[175]

3.2.1 Hydrothermal method

It is described in the literature that fullerene-semiconductor nanocomposites can be rapidly prepared by a direct hybrid method. The preparation procedure is simple and the photocatalyst is also somewhat effective. The main disadvantage is that the connection between fullerenes and inorganic semiconductors is too simple and structurally unstable, resulting in a catalytic effect that is not very stable. Bai et al [66] synthesized polyhydroxy fullerene (PHF) and TiO_2 nanocomposites by physically mixing two components in an aqueous suspension. Dispersed anatase TiO_2 nanoparticles directly in water, the TiO_2 suspension was treated under ultrasound for 30 minutes. The PHF solution was then added and mixed with the suspension for 10 minutes. However, the photocatalyst prepared by the simple mixing method did not achieve the desired catalytic effect.

Because the simple mixing methods often fail to achieve the desired experimental results, therefore, many studies no longer try this method. The hydrothermal method can obtain a well-crystallized nanomaterial at a low temperature, thereby avoiding material agglomeration and morphological changes caused by high-temperature calcination, and generally obtaining a composite material having good shape and appearance. The basic principle of hydrothermal method is dissolution-recrystallization. The high-temperature and high-pressure aqueous solution is used to dissolve a substance which is insoluble or poorly soluble

under normal conditions, or react to form a dissolved product of the substance. Crystals are precipitated by controlling the temperature difference of the solution in the autoclave to cause supersaturation. Moreover, the prepared crystals have good orientation, other substances can be uniformly doped during crystal growth, and is convenient for adjusting the ambient atmosphere during crystal formation.

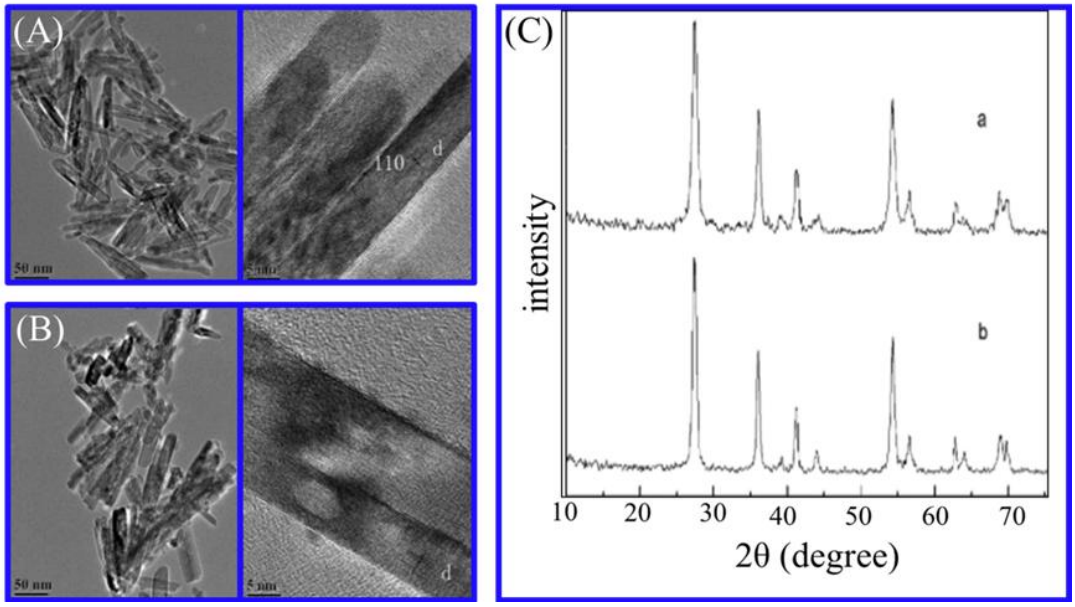

Fig. 6. (A) High-resolution (HR) TEM images of TiO_2 nanorods; (B) High-resolution (HR) TEM images of C_{60}/TiO_2; (C) XRD patterns of TiO_2 nanorods and C_{60}/TiO_2 [176]. Copyright 2009 American Chemical Society.

As mentioned above, because hydrothermal methods have these good advantages, many researchers use this method to prepare fullerene-based photocatalysts. Long et al. studied the C_{60}-doped TiO_2 nanocomposites, they used hydrothermal methods to synthesize the composite. By analyzing the XRD and TEM images, it can be known that the C_{60} cluster was successfully incorporated into the TiO_2 nanorods without changing its crystal phase (Fig.6). The experiment first

produced water-soluble C_{60}, then prepared TiO_2 nanorods, and then prepared the mixture by hydrothermal method. The optical properties of the two samples changed, absorption edges of them around 400 nm, and at the same time the band gap of TiO_2 is 3.1 ev. Through hydrothermal method the surface charge of composite substance increased , and there were some electronic interactions between them [176]. Furthermore, Ma et al. used typical hydrothermal method (453K, 24 hours) to prepare BiOCl photocatalyst modified by C_{60}, and the composite material had a microsphere structure (Fig.7A-D) .According to XRD, XPS and Raman results, we can estimate that there may be some chemical interaction between the two materials (Fig.7G,H). Compared with bare BiOCl, it could be clearly seen that the modification of BiOCl with C_{60} effectively protected the crystal phase of BiOCl, thereby improved the stability of BiOCl. And we can know that the modified catalyst morphology is completely different from the unmodified catalyst morphology, indicating that C_{60} has a profound impact on the construction of C_{60}/BiOCl microspheres, C_{60} plays a key role in regulating the growth and morphology of microsphere-like BiOCl [128].

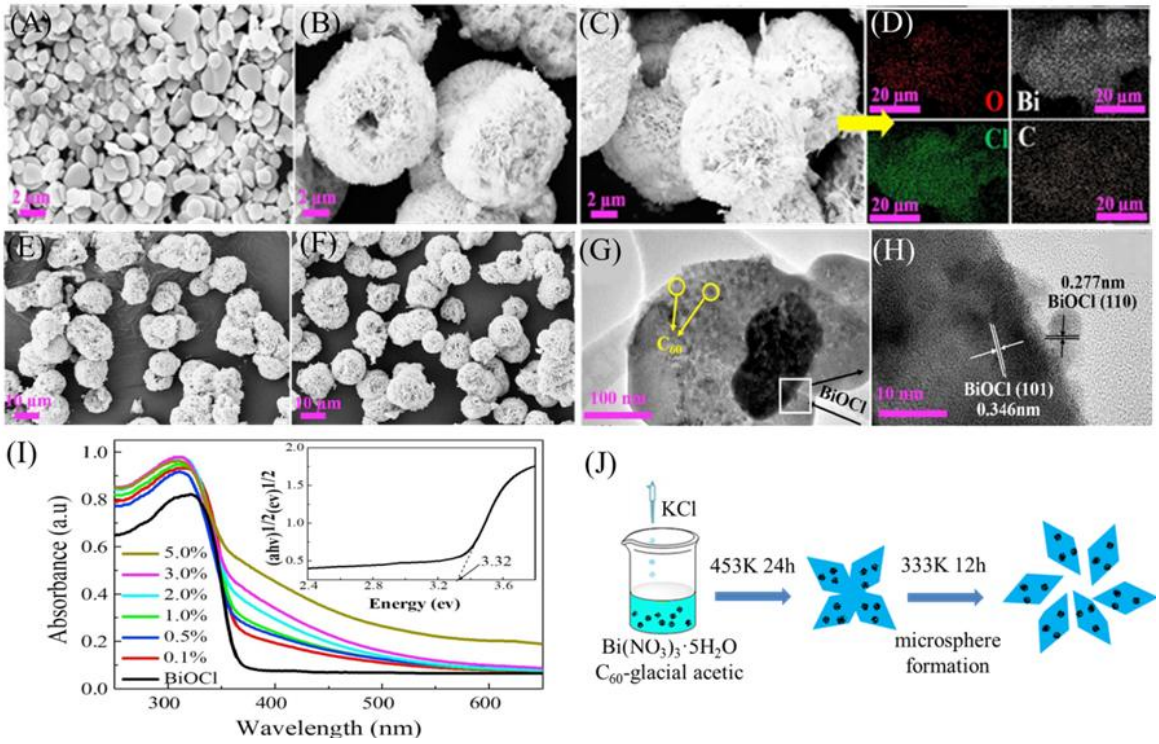

Fig.7.SEM of BiOCl (A) and 1.0% C_{60}/BiOCl (B) and (C), EDS of 1.0% C_{60}/BiOCl (D)，TEM of 1.0% C_{60}/BiOCl (E) and HRTEM 1.0% C_{60}/BiOCl (F), and XRD patterns of the C_{60}/BiOCl (G), the enlargement of [001] diffraction peak (H), UV–Vis DRS of the C_{60}/BiOCl, inset is band energy level of the bare BiOCl (I), the schematic diagram of microsphere formation (J) [128]. Copyright 2018 Elsevier.

3.2.2 Solvothermal method

The researchers developed a solvothermal method based on hydrothermal method, using organic or non-aqueous solvents as solvents, and then reacting the mixture at a certain temperature [177]. Hydrothermal method is commonly used to prepare oxide photocatalysts or some water-insensitive sulfur-containing compounds, but it is not very suitable for the preparation of water-sensitive compounds. The use

of non-aqueous solvents allows solvothermal method to expand the range of solvent-based materials. The process of preparing photocatalyst by solvothermal method is mainly divided into nucleation, dissolution, recrystallization and growth [4].

Solvothermal methods can also obtain well-crystallized nanomaterials at low temperatures, avoiding material agglomeration and morphological changes caused by high temperature calcination, and generally obtaining better morphological products. It is because of these special synthetic pathways of solvothermal method that researchers have conducted extensive explorations. Li et al. [168] synthesized a catalyst for the complexation of C_{60} with $Bi_2TiO_4F_2$ used a simple solvothermal method. The results showed that the light absorption range and photocurrent effect of the composite material was greatly enhanced. The activity of this photocatalyst was greatly improved due to the intensive interaction between the two materials and the formation of internal heterojunctions. Using lignin as a simulated pollutant, the photocatalytic degradation efficiency of C_{60} modified $Bi_2TiO_4F_2$ composite catalyst was studied by Du et al. [144]. They performed photoluminescence spectroscopy on composite materials, the results showed that the photoluminescence strength of $C_{60}/Bi_2TiO_4F_2$ was lower than other samples. In terms of optical properties, this composite absorbed light from various regions compared to its monomeric material. Qi et al. [167] successfully synthesized fullerene-modified TiO_2 composites. The method they used was also solvothermal method. C_{60} exhibited high dispersibility

and structural disorder on the composite, and did not change the crystal phase of TiO_2 with its addition. The results showed that the original catalyst was greatly changed after the addition of fullerene to the surface of the original catalyst. The band gap of the original catalyst was reduced, and an additional doping state was added. The original band gap structure was changed, thereby improved the activity of the photocatalyst and enhancing the reaction efficiency.

3.2.3 Sol-gel method

Among several synthetic methods, the sol-gel method is relatively simple. The prepared nanomaterials generally have a high purity, and the obtained catalyst has a relatively uniform particle size. Generally, the sol is prepared first, and the sol and fullerene are uniformly mixed, then aged to form a gel, and then calcined at a high temperature to form a composite material. The main disadvantage of this method is that it does not control the morphology of the material well. At present, about a quarter of the literatures on fullerene semiconductor composites are prepared by sol-gel method, of which TiO_2-C_{60} is the main one. Oh et al. [178] prepared photocatalysts of C_{60} and Vanadium-C_{60} combined with TiO_2, respectively. The method used was simple and rapid sol-gel method, the flow chart of the preparation materials was shown in the figure (Fig.8A). Structural changes and surface morphology changes of the two composites were investigated. Good dispersion of small particles on the surface of fullerenes provided many active sites (Fig.8B-D).

The C_{60}/TiO_2 composite composite consists of two phase materials, while the other nanocomposite contains a single phase (Fig.8E). Navgire et al. [162] also synthesized fullerene-doped MoO_3-TiO_2 composites by sol-gel method. The average particle size of MoO_3-TiO_2 after fullerene doping was 20 to 33 nm. It can be seen from the experimental data that the synthesized material exhibited a highly crystalline particle state. The formed material had a porous surface with small pores and a narrow band gap. The band gap of MoO_3-TiO_2 was 2.81 eV, and the band gap of fullerene-doped MoO_3-TiO_2 became 2.71 eV, and which had a significant decrease. The experiment also compared the photodegradation efficiency of these catalysts, and the latter achieved the best efficiency.

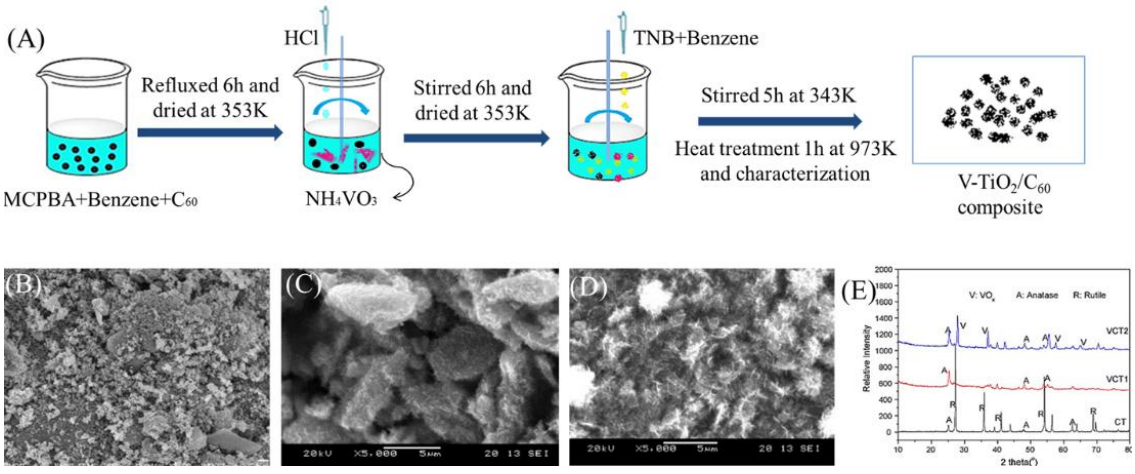

Fig.8.(A) Preparation procedure of C_{60}/TiO_2 and V–C_{60}/TiO_2 composite. SEM and FE-SEM micrographs of C_{60}/TiO_2 and V–C_{60}/TiO_2 composites: (B) CT, (C) VCT1, and (D) VCT2, (E) XRD patterns of C_{60}/TiO_2 and V–C_{60}/TiO_2 composite [178]. Copyright 2010 Elsevier.

Meng et al. also synthesized a photocatalyst of fullerene and TiO_2 composite by sol-gel method. They used titanium n-butoxide and cerium nitrate as raw materials,

and prepared the catalyst by sol-gel method and treated the fullerene with rare earth oxide. The photocatalyst had a structural morphology of uniform powder and contained aggregates of particles. From the XRD pattern of the composite nanomaterial, we know that different yttrium-doped γ-fullerene/TiO_2 prepared under this conditions exhibite anatase phase structure [113]. Meng et al. also prepared a platinum treated fullerene/TiO_2 composite. They used the same sol-gel method to synthesize the composite catalyst. Pt particles and fullerenes were combined with different functional groups, and had good and uniform distribution with TiO_2. Small particles that were well dispersed in the photocatalyst provide more reactive sites for highly polymerized reactants. The fullerene in the composite nanomaterial was well dispersed on titanium dioxide nanoparticles and had a size of about 10-20 nm [137].

3.2.4 Impregnation method

The impregnation method has the advantages of simple operation compared with the hydrothermal method, and the solvothermal method. And the catalyst nanomaterial prepared by this method has small particles and high dispersibility. Apostolopoulou et al. dispersed different quantity of C_{60} on nano-titanium dioxide to form a photocatalyst of fullerene and TiO_2 composite. Their simple continuous impregnation method was an effective synthesis method. Various types of photocatalysts were prepared by depositing different amounts of C_{60} on the titanium dioxide particles. The diffraction peak caused by anatase did not move, which

indicated that the crystal structure of the composite catalyst was the same as before. Furthermore, it was found from the experimental results that the average particle diameter of the composite catalyst particles increased as the C_{60} loading increases [157]. Grandcolas et al. first synthesized titanium nanotubes by hydrothermal method using TiO_2 powder as raw material. In the experiment, they successfully synthesized fullerene functionalized titanium dioxide nanotube composite catalyst by using impregnation method with ethanol and toluene as cosolvents. No change in morphological structure was observed in the composite photocatalyst synthesized by the impregnation method. Titanium nanotubes were loaded with 1%, 2%, and 5% C_{60} to study photocatalytic performance, respectively. Different C_{60} loadings had different nanostructures, agglomerates or assemblies of fullerenes were observed (Fig.9). When the loading of C_{60} was 1 and 2 wt%, there was no large agglomerate，a smooth and uniform distribution of "cluster" was found only in the titanium nanotubes (TiNTs) portion. However, when loading 5 wt% C_{60}, there were large agglomerates. They used photocatalytic decomposition of isopropanol to analyze the activity of photocatalysts [116].

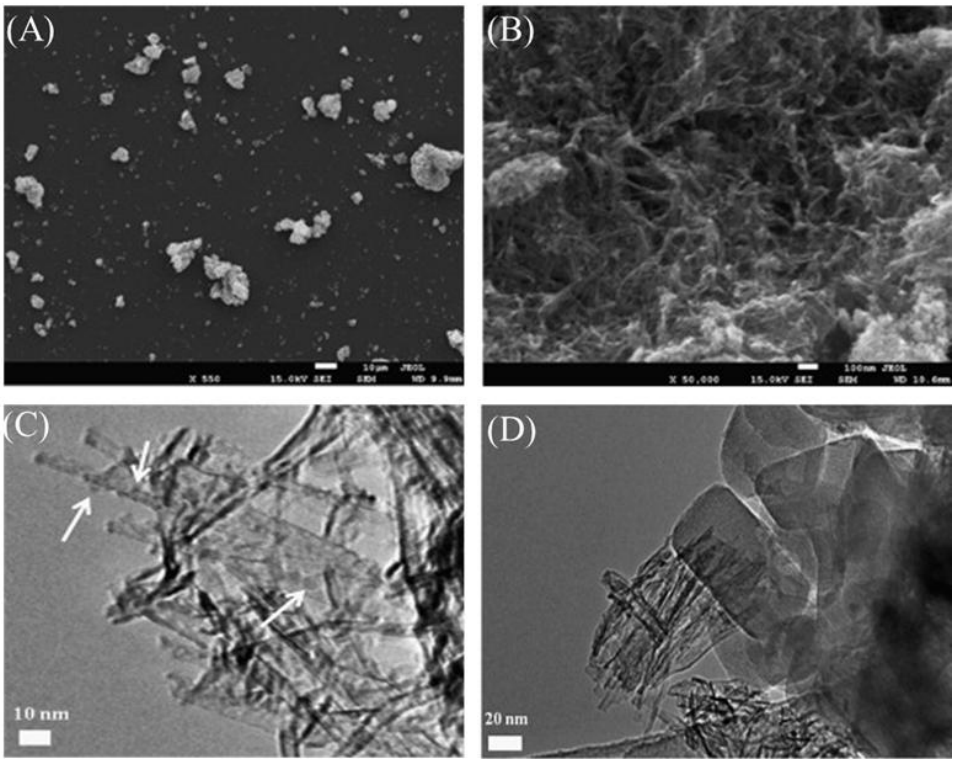

Fig. 9. (A) SEM images of the sample after hydrothermal reaction and (B) acidic rinsing showing strong agglomeration of one-dimensional nanomaterials, TEM images containing 2 wt% C_{60} (C) and 5 wt% C_{60}(D) in TiNT/C_{60} composite catalyst [116]. Copyright 2013 Elsevier.

3.2.5 Other synthesis strategy

The above several sections describe in detail several preparation methods of fullerene-based composite nanophotocatalysts, including hydrothermal method, solvothermal method, sol-gel method and impregnation method. Various preparation methods have their own advantages, and a suitable preparation process should be selected in preparing different materials. In addition to the methods we have introduced above, the researchers have tried other methods, such as chemical deposition, reprecipitation, and electrophoretic deposition technique. Abe et al. used

957 a chemical vapor deposition method to deposit C_{60} on ZnPc to prepare an organic
958 p-n double-layer photocatalytic system. This photocatalytic system took catalytic
959 degradation of N_2H_4 as the research content, generated nitrogen by decomposition of
960 the substance, and simultaneously produced clean energy hydrogen [69].
961 Arunachalam et al. synthesized cobalt nanophthalocyanine and fullerene composite
962 nanomaterials by reprecipitation method. The catalyst prepared by this method had
963 excellent performance and good morphological structure. The properties of the raw
964 materials were utilized to become visible light responsive photocatalysts. The
965 composite nanophotocatalyst nanocomposite exhibited superior photocatalytic
966 activity than single nanoparticles and AlPc-based composites [70]. Chai et al.
967 successfully prepared fullerene-modified C_3N_4 nanocomposites, which could exert
968 high activity under experimental lighting conditions. The photocatalyst was prepared
969 by an adsorption method, it was convenient and simple to synthesize. Carbon nitride
970 had a two-dimensional layered structure (Fig. 10A, B).The dispersion of fullerenes
971 in the prepared composites was very well (Fig. 10D), and its addition did not change
972 the crystal lattice and morphology of the carbon nitride (Fig. 10E). The results
973 showed that when the amount of fullerene in the composite nanomaterial was 1 wt%,
974 the photocatast reached the optimal activity [130].

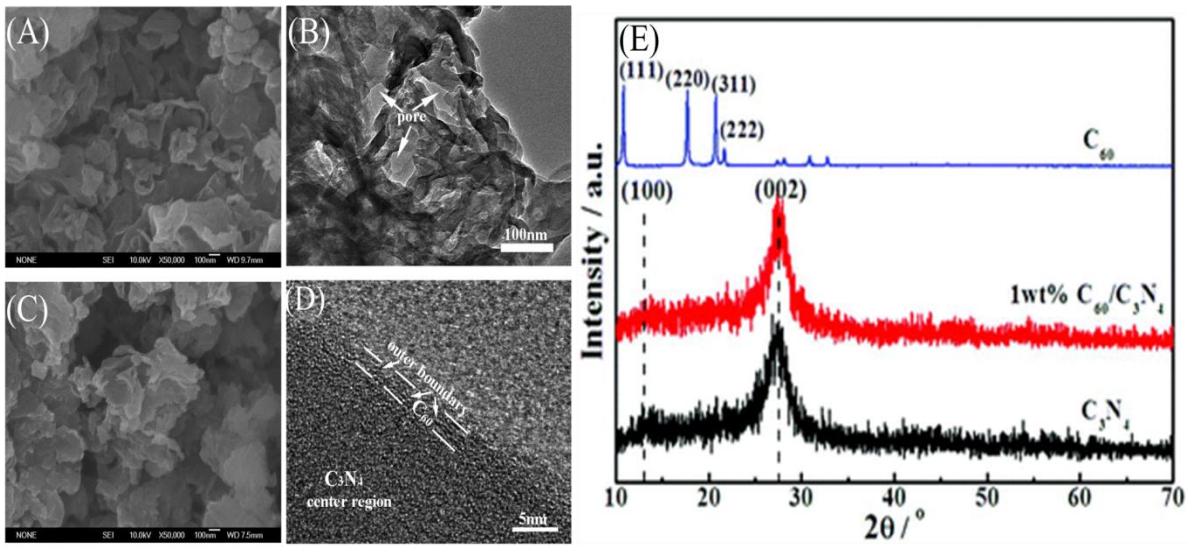

Fig. 10. (A) SEM images of bare C_3N_4, (B) SEM images of 1 wt% C_{60}/C_3N_4 composite ,(C-D) TEM inages of 1 wt% C_{60}/C_3N_4 composite,(E) XRD patterns of bare C_3N_4,C_{60} and 1 wt% C_{60}/C_3N_4 composite [130]. Copyright 2014 Royal Society of Chemistry.

Lin et al. used electrophoretic deposition technology to prepare nano-photocatalysts with fullerene and TiO_2 nanotube array composites. C_{60} on the composite increased the photocatalyst charge separation process, promoted the transfer of electrons and affected the interaction between the electronic layers importantly [126]. Ju et al. synthesized a C_{60}@AgCl nanoparticle photocatalyst supported by ZnAlTi layered double oxide by coprecipitation-photoinduced method (Fig. 11A). The researchers quantitatively analyzed the degradation of bisphenol A during the experiment. The pore size distribution of the catalyst was evenly distributed. In the simulated visible light environment, the maximum degradation efficiency of bisphenol A was 90% (Fig. 11B), which showed that the removal of the pollutant by the catalyst did have a good effect [143]. The possible reaction pathway

for bisphenol A (BPA) degradation was shown in the figure (Fig. 11C).

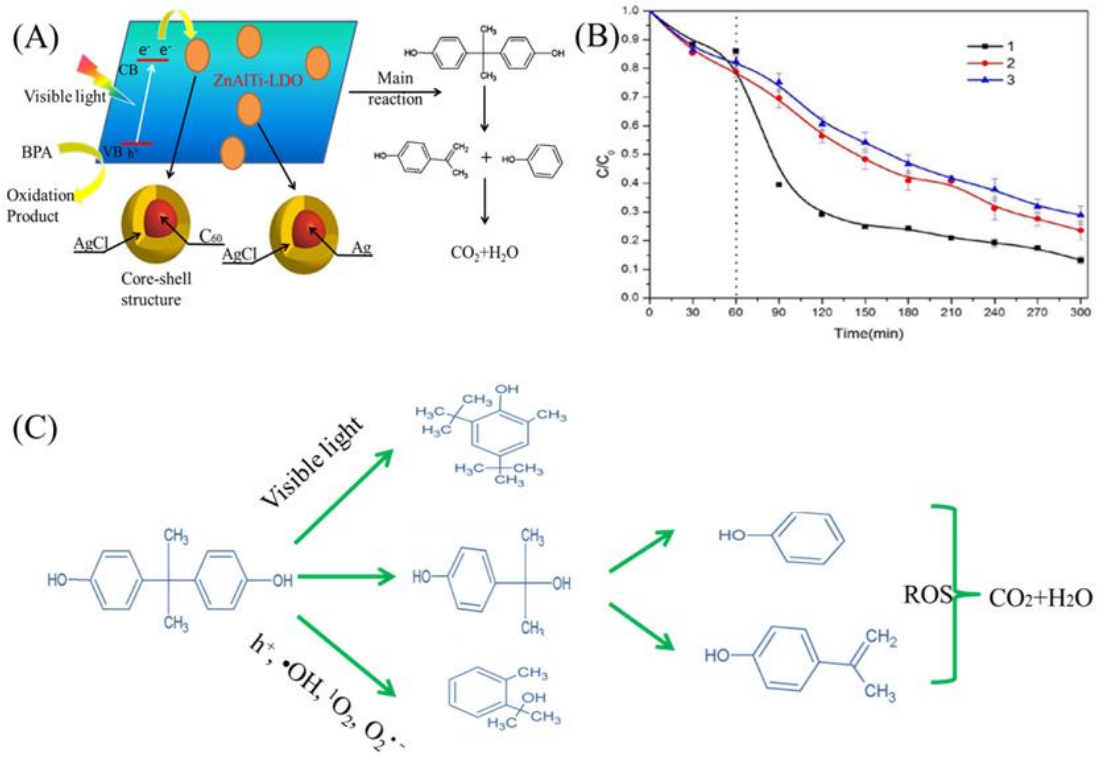

Fig. 11. (A) Schematic drawing illustrating synthetic route and the mechanism of charge separation and photocatalytic process over C_{60}@AgCl-LDO (layered double oxide) photocatalysts under visible light irradiation. (B) Degradation of BPA in consecutive runs using the recycled C_{60}@AgCl-LDO [143]. (C) The possible reaction pathway for BPA degradation. Copyright 2018 Elsevier.

4. Application of fullerene modified photocatalyst

In recent years, photocatalysts prepared by combining fullerenes and their derivatives with inorganic semiconductor materials and organic materials have made great progress. They have extensive applications in photocatalysis, and achieved

outstanding achievements in the environment, energy and other areas through photocatalytic reactions. The current researches are mainly focused on environmental modification, such as the degradation of water pollutants, sterilization and disinfection. Energy production applications, such as hydrogen production, organic synthesis, etc. Many studies have shown that the reactivity of fullerene composites is enhanced compared to pure inorganic materials, and has broad application prospects.

4.1 Environmental modification

4.1.1 Degradation of water pollutants

There are many kinds of pollutants in water, typically, such as organic dyes, persistent organic pollutants, and heavy metal ions are widely studied in the field of photocatalysis [179]. Photocatalytic applications of fullerene photocatalysts in the degradation of organic pollutants were shown in Table 2.

Among these pollutants, organic dyes are typical simulated pollutants in many literatures, and the application of photocatalysts based on fullerenes and their derivatives in photocatalytic degradation of dyes has been studied. Bai et al. used a simple conventional heat treatment method to synthesize composite nanomaterials of fullerene C_{60} and graphite phase carbon nitride. Compared with the pure carbon nitride catalyst, the activity of the composite photocatalyst to degrade the organic dye methylene blue and phenol pollutants are rapidly improved after C_{60}

modification. By combining the fullerene with a carbon nitride matrix, the valence band of carbon nitride changed to some extent, and the valence band energy became lower, which provided strong photooxidation under visible light (Fig.12). The photocatalyst composite had many advantages in the catalytic process that organic compounds can be rapidly oxidized and removed [72]. The mechanism diagram of charge separation and photocatalysis process were shown in the figure (Fig.12E). C_{60}-incorporated TiO_2 nanorods were prepared by Long et al. [176] they found that the photocatalyst had high degradation efficiency for rhodamine B. After 1.5 h of reaction, the degradation efficiency was basically 99%.

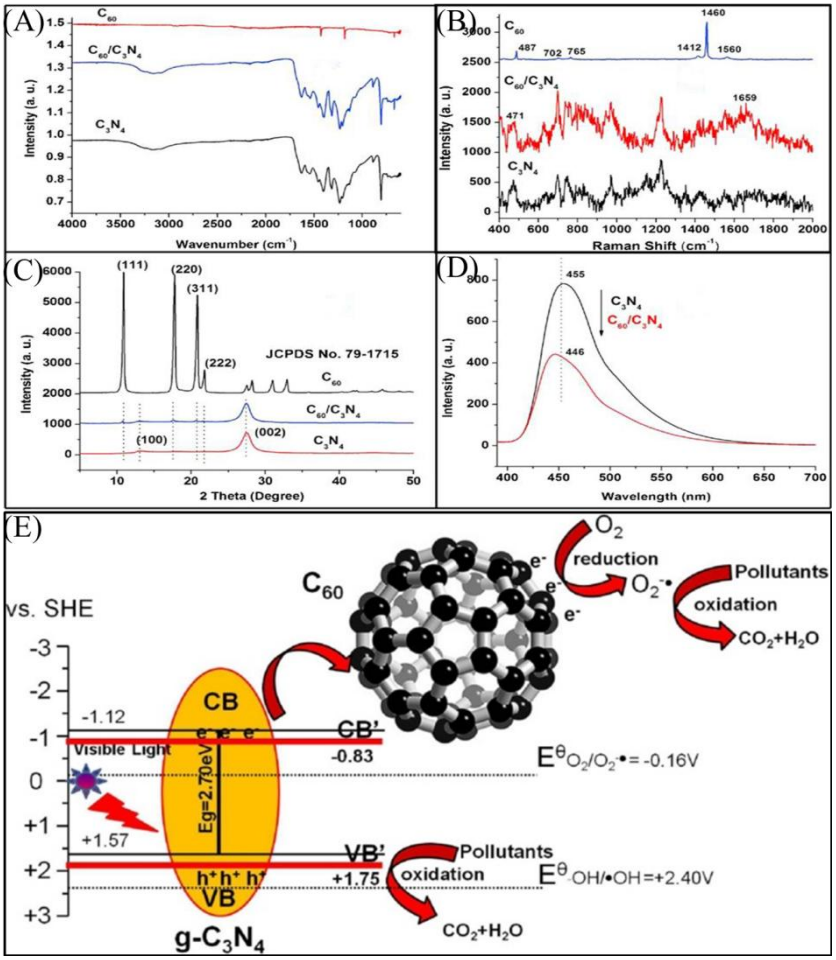

Fig.12. (A) FTIR spectra of g-C_3N_4 and C_{60}/g-C_3N_4 photocatalysts; (B) Raman spectra of g-C_3N_4 and C_{60}/g-C_3N_4 photocatalysts; (C) XRD patterns of g-C_3N_4 and C_{60}/g-C_3N_4 photocatalysts; (D) Room-temperature PL excitation and emission spectra of g-C_3N_4 and C_{60}/g-C_3N_4photocatalysts (ex = 370 nm); (E)Schematic diagram of the mechanism of charge separation and photocatalysis of C_{60}/g-C_3N_4 photocatalyst [72]. Copyright 2014 Elsevier.

The combination of experimental and theoretical calculations can help us to have a better understanding of the inherent mechanism of composite photocatalysts. Ding et al. studied the intrinsic mechanism of C_{60} modified SnO_2 composite photocatalyst by density functional theory [180]. Firstly, the C_{60}/SnO_2 (101) heterostructure was geometrically optimized (Fig.13A). The almost unchanged structure of the optimized C_{60} and SnO_2 (101) surfaces indicated that the interfacial interaction is indeed a vdW force rather than a covalent. They first calculated the molecular energy levels of C_{60} to verify the validity of the calculations, as shown in Figure 13B. The charge density of the interface region changes significantly (Fig.13C), which indicates that the effect of interfacial interaction on C_{60} charge redistribution is much greater than that of SnO_2 (101) surface. In the C_{60}/SnO_2 (101) heterostructure, the strong charge accumulation (blue part) is found mainly on the O atoms and the C atoms, and the charge depletion (yellow part) is mainly present on the C atoms. More importantly, the redistribution of charge causes the C atoms (at C_{60} top) to be negatively/positively charged, becoming an active site during the reaction, thereby increasing photocatalytic efficiency. The surface state (Fig.13E)

(has a significant effect on the properties of the materials) is formed at the bottom of the SnO_2 CB to reduce the band gap of the SnO_2 (101) surface to 1.76 eV, as shown in Fig. 13D. The VB top and CB bottom of the C_{60}/SnO_2 (101) heterojunction are consist of C 2p and Sn 5s orbitals (Fig.13F), respectively.

As is apparent from Fig. 1G, a type II heterojunction was found in composite C_{60}/SnO_2. C_{60} acts as a sensitizer on the surface of SnO_2 (101) to enhance the separation of electron-hole pairs in the photocatalytic process. They used Mulliken population analysis to quantitatively analyze charge changes at the interface (Fig.13H), which indicated that the modification of C_{60} increased the electrons of the O atom and the Sn atoms lost more electrons in the composite than monomer. Due to the interaction between the surface of C_{60} and SnO_2, the interface charge distribution fluctuates, which will change the electrostatic potential distribution at the interface. The potential on the plane of the Sn atoms is larger than that of the C atoms, causing a large potential difference between them. The huge intrinsic potential prevents the recombination of photogenerated charge carriers, thereby enhancing the photocatalytic activity of C_{60}/SnO_2 heterostructures.

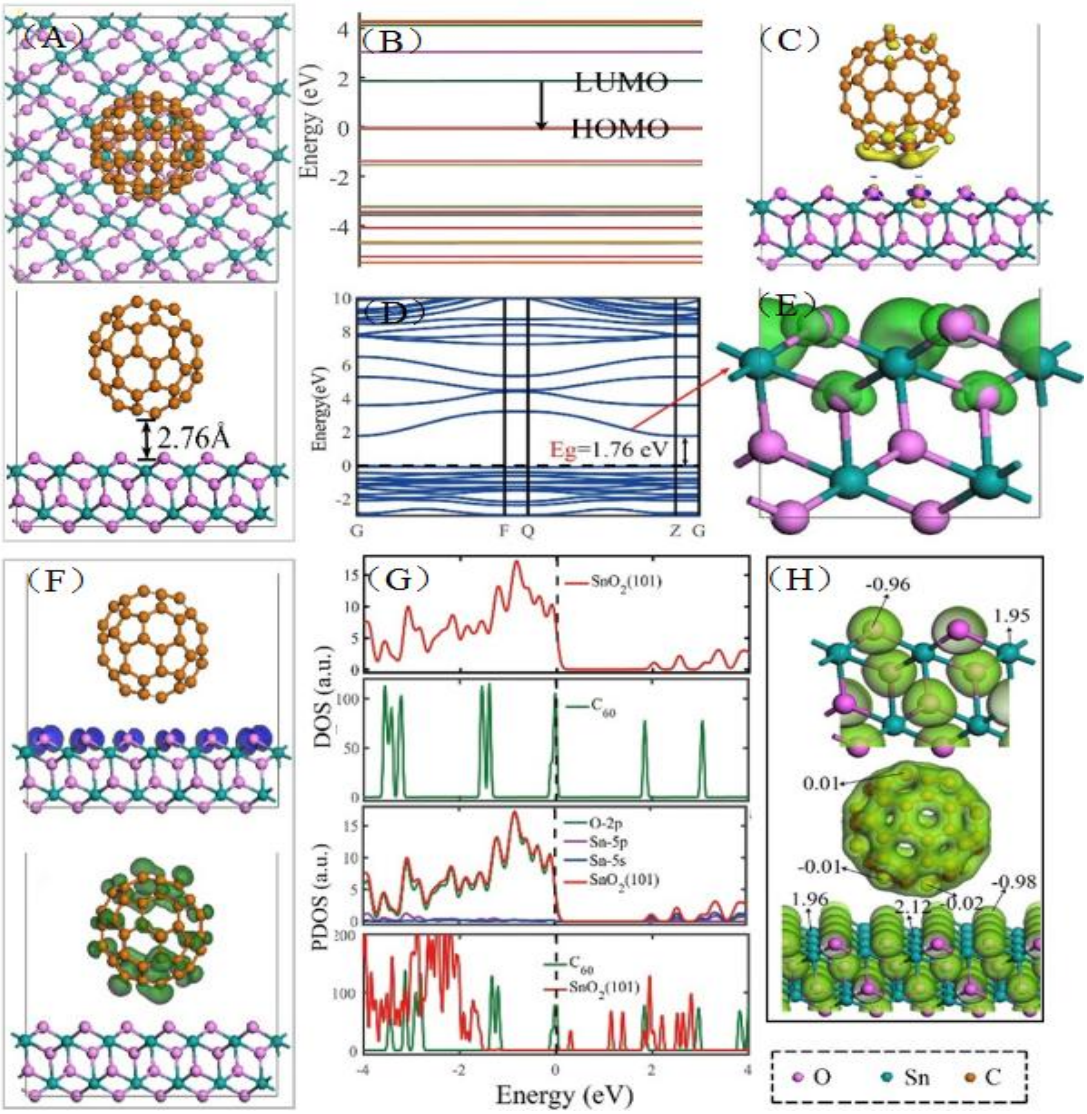

Fig.13. (A) Top view and side view of the C_{60}/SnO_2 (101) model, (B) Molecular energy levels of C_{60}.(C) The 3D charge density differences for C_{60}/SnO_2 (101), the blue and yellow represent charge accumulation and depletion in the space, respectively. (D) Band structures for SnO_2 (101). (E) The electron and hole density distributions for SnO_2 (101) surface states. (F) Side views of the electron and hole density distributions for the LUL and HOL for the C_{60}/SnO_2 (101), respectively. (G) The total density of states for SnO_2 (101) and C_{60}, and the local density of states for SnO_2 (101) and C_{60}/SnO_2 (101), respectively. (H) The charge distribution maps of SnO_2 (101), and C_{60}/SnO_2 (101) [180]. Copyright 2017 Elsevier.

1077 Table.2. Photocatalytic application of fullerene-based photocatalysts in organic pollutants degradation (N/A = not applicable).

Photocatalyst	Preparation method	Fullerene content [wt%]	Incident light	Light intensity	Degraded substance	BET (m^2/g)	Efficiency	Enhancement factor	Ref
$TiNTs/C_{60}$	impregnation	5	$\lambda > 420$ nm	300W Xe lamp	Isopropanol	290	99.9%(11 h)	2 times than TiNTs	[116]
TiO_2/C_{60}	deposition	N/A	UV	18 W UV-A blacklights lamp	methyl orange	-	-	-	[124]
TiO_2/C_{60}	solution	N/A	UV	8 W mercury lamp	methylene blue	-	99.5%(1 h)	-	[125]
TiO_2/C_{60}	solvothermal	2	UV-A	8 W medium-pressure mercury lamp	methylene blue	133.60	99.9%(1 h)	1.43 times than TiO_2	[167]
TiO_2/C_{60}	adsorption	2.5	$\lambda = 254$ nm	11W germicidal lamp	salicylic acid	53	90%(2 h)	1.63 times than TiO_2	[181]
SiO_2/C_{60}	evaporation	N/A	$\lambda > 420$ nm	300W xenon lamp	methyl orange	-	96%(25 min)	-	[141]
C_3N_4/C_{60}	adsorption	1	$\lambda > 420$ nm	500 W xenon lamp	rhodamine B	-	97%(1 h)	1.8 times than C_3N_4	[130]
$BiOCl/C_{60}$	hydrothermal	1	Visible	500 W Xe lamp	rhodamine B	19.4	99.7%(12 h)	9 times than BiOCl	[128]

$Bi_2TiO_4F_2/C_{60}$	solvothermal	N/A	Visible	500 W xenon lamp	lignin	-	-	-	[144]
LDO-AgCl/C_{60}	coprecipitation	N/A	Visible	300W xenon lamp	Bisphenol A	15.27	90%(5 h)	2.17 times than LDO	[143]
$Bi_2TiO_4F_2/C_{60}$	solvothermal	1	$\lambda > 420$ nm	500 W Xenon lamp	Rhodamine B	25.4	90%(2 h)	1.5 times than $Bi_2TiO_4F_2$	[168]
$WO_3/TiO_2/C_{60}$	sol-gel	2	Visible	8 W halogen lamp	methylene blue	49.21	-	-	[142]
$Pt/TiO_2/C_{60}$	sol-gel	N/A	Visible	8 W halogen lamp	methyl orange	31.7	80%(2 h)	1.63 times than TiO_2	[137]
SiO_2/C_{60}	impregnation	3	$\lambda > 420$ nm	150W xenon lamp	heptene	194	95%(100 min)	-	[129]
Ag_3PO_4/C_{60}	impregnation	2	Visible	500W Xe lamp	acid red 18	-	90%(1 h)	3.5 times than Ag_3PO_4	[159]
Bi_2MoO_6/C_{60}	hydrothermal	3	$\lambda > 420$ nm	500 W Xe lamp	bromate ions	3.50	92%(2 h)	1.3 times than Bi_2MoO_6	[166]
Fe_2O_3/C_{60}	impregnation	N/A	$\lambda > 420$ nm	300 W UV-vis lamp	phenol	-	98.9%(80 min)	-	[160]

Xu et al. found that C_{60}/Ag_3PO_4 composites were synthesized by modification of Ag_3PO_4 with acid-treated fullerene (C_{60})(Fig. 14A). Pure Ag_3PO_4 had an irregular mixed form (such as tetrahedral, spherical) with a smooth surface, but the introduction of C_{60} controlled the growth of Ag_3PO_4 particles (Fig. 14B,C). It was found that the optimum C_{60} content in the composite was 2%, and the superoxide radicals were most produced, which played a major role in photodegrading acid red 18 (Fig. 14E). The degradation rate of acid red 18 (AR18) was much improved quickly, almost 3.5 times of the degradation rate without modification, and the removal efficiency of AR18 was 90% after 60 minutes of reaction (Fig. 14D) [159]. The detailed photo-degradation reaction processes were as follows:

$$Ag_3PO_4 + hv(visiblelight) \rightarrow e^- + h^+ \quad (1)$$

$$C_{60} + hv(visiblelight) \rightarrow {}^1C_{60}{}^* \rightarrow {}^3C_{60}{}^* \quad (2)$$

$${}^3C_{60}{}^* + e^- \rightarrow C_{60}{}^{\bullet-} \quad (3)$$

$$C_{60}{}^{\bullet-} + e^- \rightarrow C_{60} + O_2{}^{\bullet-} \quad (4)$$

$$O_2 + e^- \rightarrow O_2{}^{\bullet-} \quad (5)$$

$$H_2O + h^+ \rightarrow \cdot OH + H^+ \quad (6)$$

$$O_2{}^{\bullet-} + h^+ \rightarrow O_2{}^1 \quad (7)$$

$$AR18 \xrightarrow{O_2{}^{\bullet-} or \bullet OH or O_2{}^1 or h^+} CO_2 + H_2O \quad (8)$$

In addition to organic dyes, some researches are to treat other important pollutants in water, namely organic pesticides and heavy metal ions. Djordjevic et al. [67] used fullerene and tetrahydrofuran nanoparticles to modify the TiO_2 catalyst to produce a material with superior properties . It was found that the TiO_2/fullerenol

$C_{60}(OH)_{24}$ nanoparticles (FNP) system was best for simulating the decline of sunlight and removing the herbicide mesotrione. For the purpose of preventing recombination of charge during photocatalytic reaction, the author added H_2O_2 and $KBrO_3$ to the solution, which are capable of accepting electrons as electron acceptors, and concluded that the degradation of the first phase substrate may be carried out by hydroxyl radicals. The reaction mechanism was mainly through pores after 60 min irradiation. Kanchanatip et al. [148] synthesized V-TiO_2 and C_{60}/vanadium (V)-TiO_2 anatase photocatalysts with titanium isopropoxide (IV) to degrade pesticide paraquat under visible light. The catalyst obtained by the combination of 1 wt% C_{60} and 1 wt% V-TiO_2 exhibited the optimal performance, the kinetic rate constant of photocatalytic degradation reached a maximum, and the degradation process was in an optimal state. Park et al. [108] used water-soluble fullerol ($C_{60}(OH)_x$) to activate titanium dioxide under visible light to prepare a composite catalyst, which had a good effect on the reduction of toxic Cr^{VI} in water to less toxic Cr^{III}.

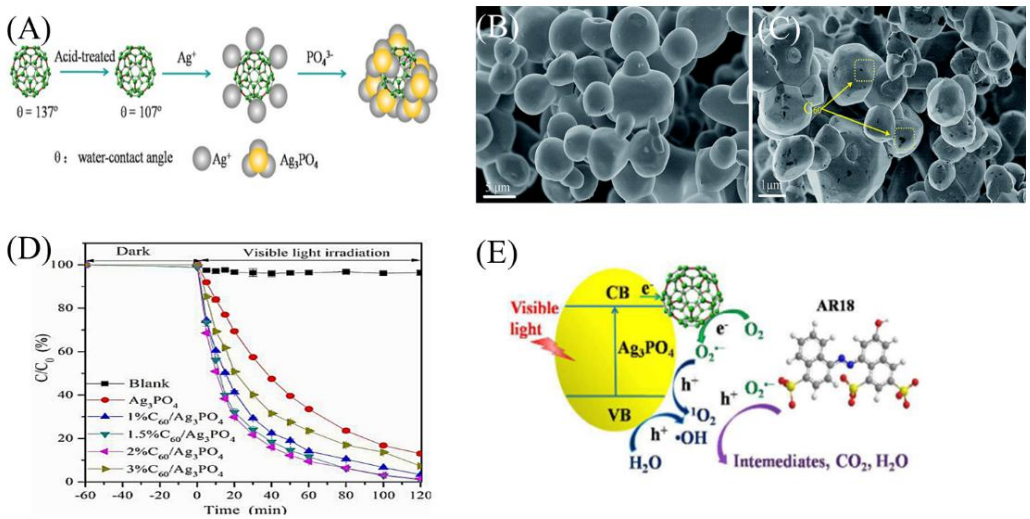

Fig. 14. (A) Schematic illustration of the synthesis of C_{60}/Ag_3PO_4, SEM images of the various samples. (B) Ag_3PO_4; (C) $2\%C_{60}/Ag_3PO_4$; (D) Decolorization of acid red 18 under different conditions. (E) Photocatalytic mechanism of organics degradation over C_{60}/Ag_3PO_4 composite [159]. Copyright 2016 Royal Society of Chemistry.

Qi et al [167]. proposed the C_{60}/a-TiO_2 shows remarkably enhanced organic dyes degradation activity. DFT calculations were used to examine the interaction between the C_{60} and a-TiO_2 surface to obtain a further understanding of the C_{60}@ a-TiO_2 (101) interface (Fig.15). The calculated adsorption energy indicated that C_{60} had a strong covalent interaction with the surface of a-TiO_2 (101) by COOH hybridization. The projected density of states (PDOS) of the C_{60}-COOH @ a-TiO_2 (101) interface and clean a-TiO_2 (101) surface were calculated (Fig. 15E, F) to investigate how the C_{60} derivative influences the electronic structure of the surface of a-TiO_2 (101). Figure 2E illustrated the clean a-TiO_2 (101) surface band gap energy was 1.9 eV. The valence band maximum (VBM) and the conduction band minimum (CBM) were mainly composed of O 2p orbital and Ti 3d states, respectively. Figure 2F was the top of the C_{60}-COOH@a-TiO_2 (101) valence band and belongs to C_{60}-COOH 2p. The bandgap was reduced to 0.8 eV after the introduction of the intermediate state, resulting in an enhanced light absorption spectrum of the heterojunction. The researchers gave a photocatalytic enhancement mechanism from the calculation results (Fig.15G). On the one hand, C_{60} has the ability to accelerate electron transfer and improve charge separation efficiency, and on the other hand, it has strong light absorption capacity.

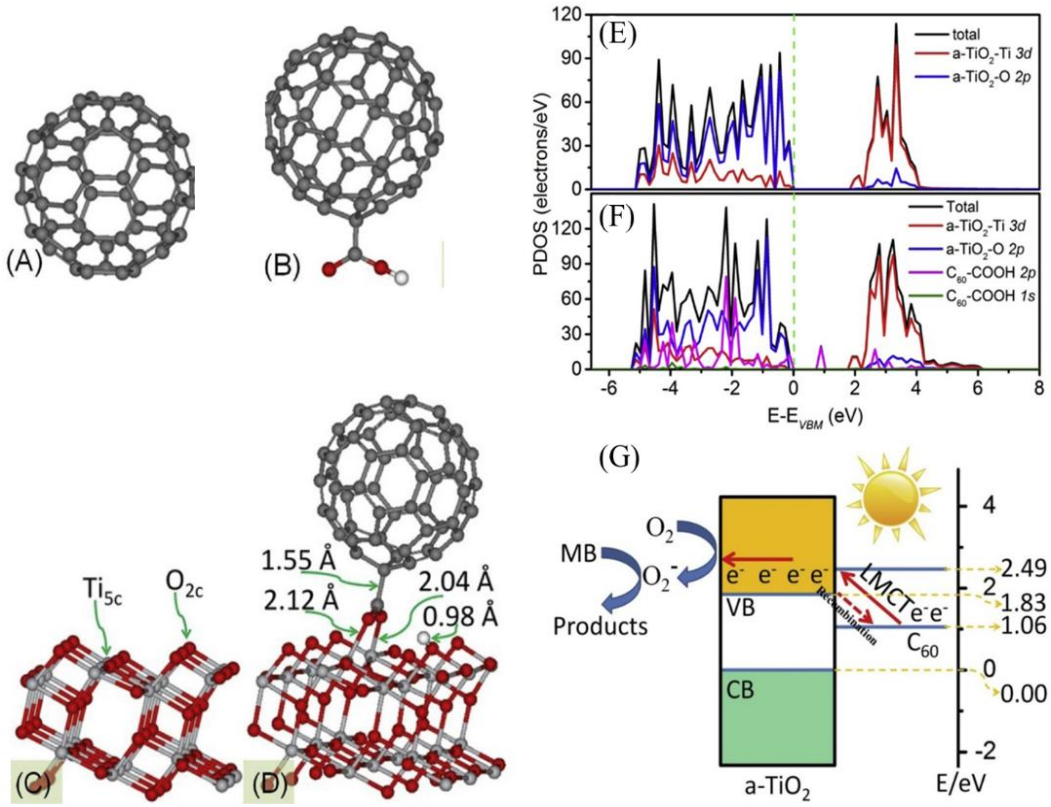

Fig.15. DFT optimized structures of (A) C_{60}, (B) C_{60}-COOH, (C) clean a-TiO_2(101) and (D) C_{60}-COOH@a-TiO_2(101). PDOS of (E) clean a-TiO_2(101) and (F) C_{60}-COOH@a-TiO_2(101). (G) Illustration of the photocatalytic degradation mechanism of MB over C_{60}@a-TiO_2 [167]. Copyright 2016 Elsevier.

4.1.2 Sterilization and disinfection

In the process of water treatment, not only the chemical pollutants in the water need to be removed, but also microbial pollutants, such as pathogens and bacteria need to be removed to ensure the water body is completely purified. Most photocatalysts can be used as antibacterial agents and disinfectants in water under appropriate light irradiation, while fullerene/semiconductor composite photocatalysts exhibit better antibacterial properties. Choi et al. [112] synthesized a

catalyst composite system composed of C_{60} aminofullerene and functionalized mesoporous silica-coated magnetite nanoparticles as magnetic separation carriers (Fig. 16A,B). The catalyst could inactivate MS-2 phage, mainly because of C_{60} light-induced singlet oxygen production after illumination. In dark conditions, the activity of the virus was still very strong, but it was well suppressed after 80 minutes (Fig. 16C). Moor et al. [182] demonstrated the production of singlet oxygen and the inactivation of MS-2 phage by silica loaded fullerene composites (Fig.16D). Sepahvand et al.prepared a fullerene-modified magnetic silver phosphate composite ($Ag_3PO_4/Fe_3O_4/C_{60}$), which had high-efficiency photocatalytic activity [58]. The researchers found that the composite photocatalyst had good antibacterial activity against several pathogenic bacteria in human body. The bactericidal mechanism of m-Ag_3PO_4/C_{60} nanocomposite was mainly adhered to the surface of negatively charged bacterial cells, which changed the characteristics of the cell membrane and cell wall. It inhibited important cell functions such as permeability, osmotic regulation, electron transfer and respiration, and can also release silver ions, resulting in an enhanced bactericidal effect.

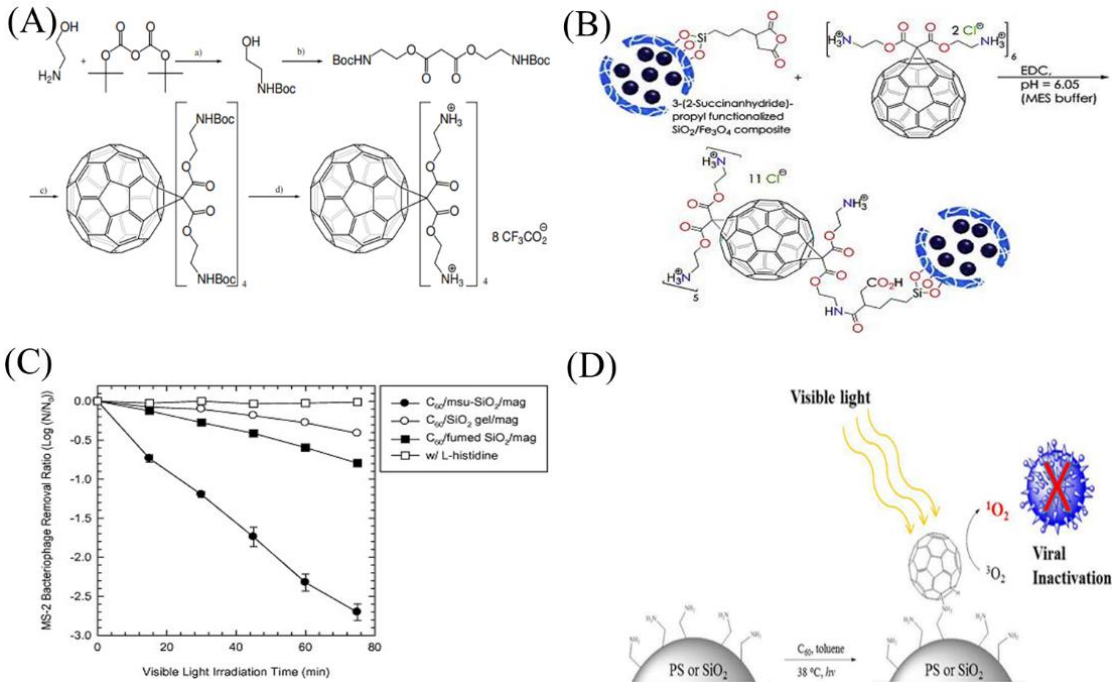

Fig. 16. (A) Formation mechanism of amino fullerenes [183]. Copyright 2009 American Chemical Society. (B) Immoblization of C_{60} aminofullerene on functionalized magnetic silica composite; (C) MS-2 bacteriophage inactivation by C_{60}/msu-SiO_2/mag, C_{60}/SiO_2 gel/mag, and C_{60}/fumed SiO_2/mag under visible-light irradiation [112]. Copyright 2014 Elsevier. (D) The schematic diagram of solid supported fullerene materials [182]. Copyright 2014 American Chemical Society.

Most photocatalysts that have demonstrated antiviral activity contain (heavy metal) metals, which are potentially hazardous. It is particularly important to explore new safe photocatalysts for bacterial and viral disinfection. A good method for preventing the low water solubility of materials by combining C_{60} with hydrophilic groups and water-soluble C_{60} derivatives are also being studied as a photocatalyst for antibacterial antivirus. Bai et al. [66] developed a fullerene-based photocatalytic coating material for the effective killing of microorganisms by physically mixing

two components in an aqueous suspension to synthesize polyhydroxy fullerenes and TiO_2 nanocomposites (Fig. 17A). This nanocomposite was used for photocatalytic removal of *Aspergillus niger,* and the clearance rate of this fungus was used as a reference index (Fig. 17B). The nanocomposite inactivated spores three to four times faster than the bactericidal rate of the TiO_2 coating without polyhydroxyfullerene. Krishna et al. [107] used polyhydroxy fullerene to increase the photocatalytic degradation rate of titanium dioxide. The composite catalyst had a good inactivation effect on *Escherichia coli*. The *E. coli* inactivation rate coefficient of P25 and polyhydroxyfullerene composite catalyst was about twice than that of P25 catalyst alone. Moor et al. [182] demonstrated the production of singlet oxygen and the inactivation of MS-2 phage by silica loaded fullerene composites. Moor et al. [74] prepared a mesoporous silica support MCM-41, which was used as a base for fullerene composites to form a composite nanomaterial (Fig. 18A). The resulting composite nanomaterial exhibited significant photoactivity. SEM and TEM images of C_{70}/MCM-41were shown below (Fig. 18B,C). The results of these experiments showed that the composite nanomaterial can rapidly inactivate MS-2 phage in sunlight and oxidize various organic pollutants without being contaminated (Fig. 18D). These excellent properties reflected the value of these materials in practical applications. In general, these materials are easy to synthesize and have significantly enhanced visible light activity. Based on these characteristics, the application of fullerene nanomaterials in water treatment sterilization and disinfection technology is expanded.

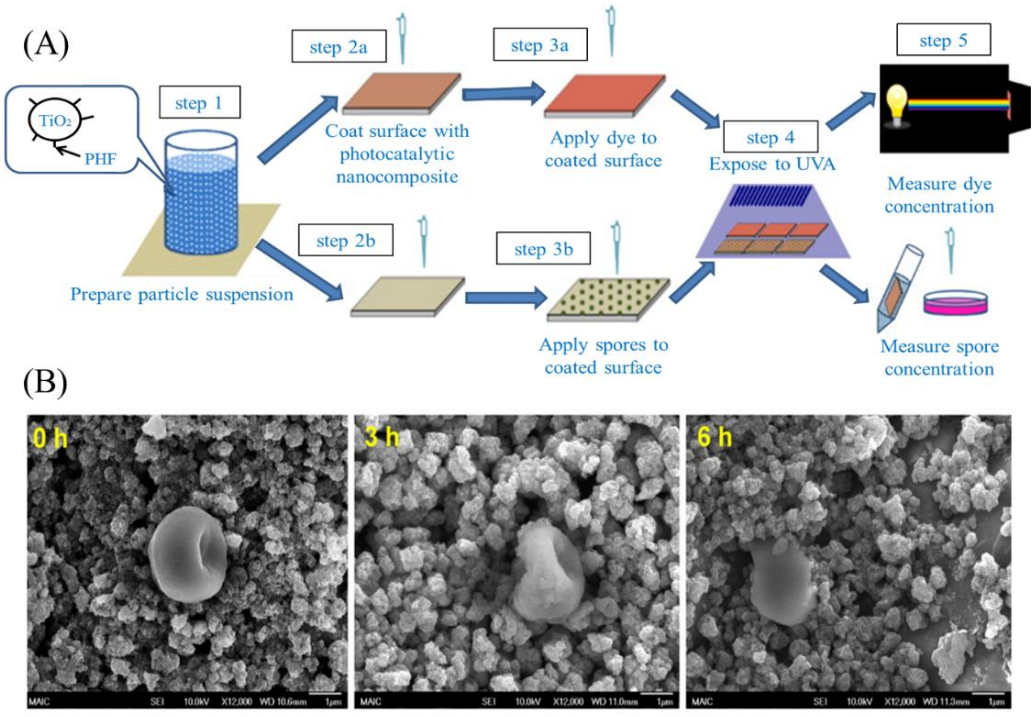

1202

1203 Fig. 17. (A) Procedure for testing performance of photocatalytic coatings, (B) changes in the

1204 morphology of virus spores inactivated by C_{60}/TiO_2 at different times [66]. Copyright 2012

1205 Elsevier.

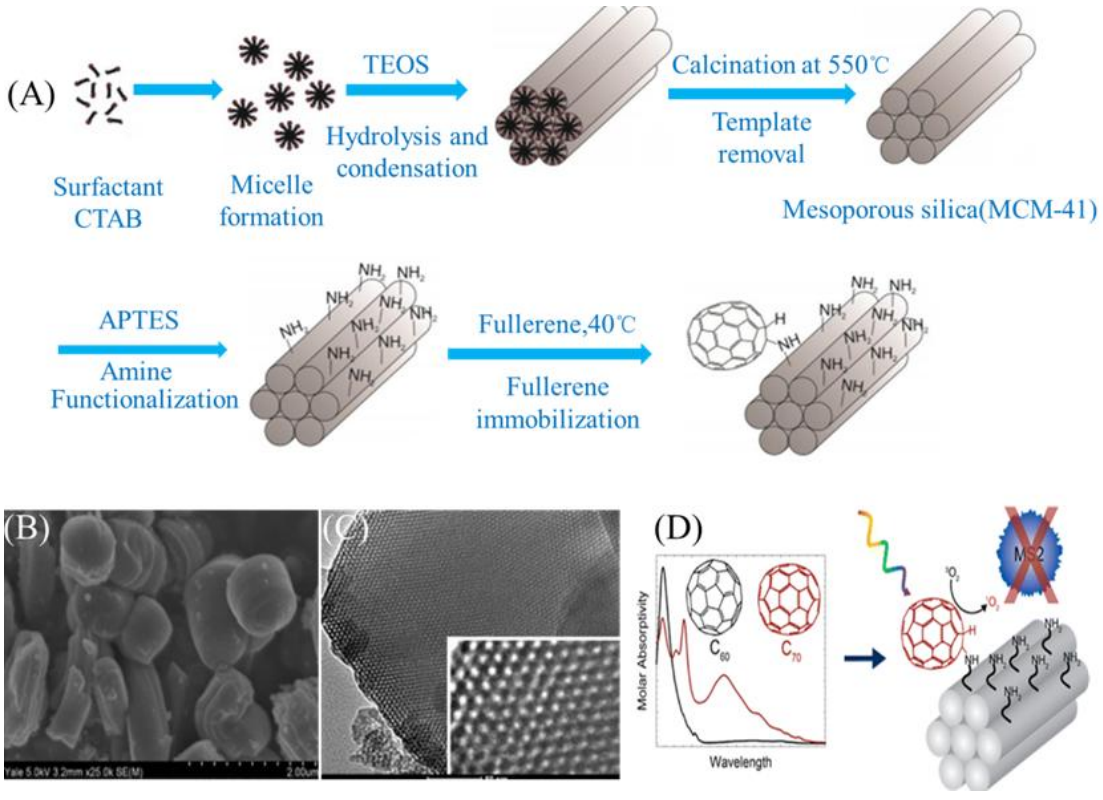

1206

Fig. 18. (A) General synthesis method employed outlining the preparation of MCM-41, functionalization introducing terminal amine groups, and finally fullerene immobilization. (B) SEM images of C_{70}/MCM-41. (C) TEM images of C_{70}/MCM-41. (D) UV/vis spectrum of fullerenes and virus inactivation of C_{70}/SiO_2 catalyst [74]. Copyright 2015 American Chemical Society.

4.2 Organic synthesis and decomposition

Many organic substances have great applications in environmental pollution control, some of which are used as adsorbents [184], some as surfactants [185-187], and so on. Therefore, their high-efficiency synthesis also has certain research value, and photocatalysis technology has important applications in the synthesis and decomposition of organic matter. Photocatalysts based on fullerenes and their derivatives have great applications not only in the degradation of water pollutants, but also in organic synthesis and decomposition. Huang et al. [71] used a C_{60}-Bodipy complex catalyzed cycloaddition reaction of organic compounds. The composite catalyst had the characteristics of strong absorption of light and stability. This experiment was of great significance for exploring new organic photosensitizers and photocatalysts for catalyzing organic reactions. Sepahvand et al. [58] studied the catalytic reduction of 4-nitrophenol (4-NP) by $Ag_3PO_4/Fe_3O_4/C_{60}$ nanocomposites. The results showed that the yield of the product in the aqueous solution of $NaBH_4$ was 98%. In the catalytic reaction, $Ag_3PO_4/Fe_3O_4/C_{60}$ nanocomposites exhibited higher catalytic activity than pure Ag_3PO_4. When used for

organic decomposition, photocatalysts based on fullerenes and their derivatives tended to mainly act on catalytic decomposition of olefins. Kyriakopoulos et al. [134] prepared a photocatalyst of MCM-41 and fullerene C_{60} composite, which was used for the oxidation of olefins to corresponding hydroperoxides. Small crystal of C_{60} had high dispersion on the surface of composite catalyst. Panagiotou et al. [129] effectively dispersed C_{60} on the surface of silica gel. They used the composite catalyst to decompose 2-methyl-2-heptene and tested the performance of the catalyst with its degradation effect. After the catalyst was added, the conversion rate of the organic matter was greatly increased until the amount of C_{60} was increased to 3% (w/w) and then decreased, and the number of conversions and the switching frequency were always lowered, indicating the best C_{60} load was 3%. Tzirakis et al. [161] immobilized fullerene C_{60} on the surface of γ-Al_2O_3. It was a novel heterogeneous catalyst for the oxidation of certain organics in an oxygen atmosphere. The catalytic activity of the substrate increased with the content of fullerenes during the experiment process. However, the activity of the catalyst decreased when the amount of C_{60} reached 3% (w/w).

4.3 Hydrogen production

Energy issues are the focus of attention in this century. Access to clean energy is a common dream of mankind. Since TiO_2 was found to be capable of photolysis of water to produce hydrogen in 1972 [5], people have never stopped exploring the path of hydrothermal hydrogen production. The production of clean energy through

photocatalytic reactions also attracted a lot of attention. The applications of fullerene-based photocatalysts in hydrogen production were shown in Table 3.

New materials are constantly being researched to improve the efficiency of photohydrolysis of hydrogen, not just titanium dioxide. Fullerenes exhibited a certain application value in the field of photolysis of water to hydrogen. Song et al. [164] prepared nanomaterials composite of fullerene/graphene/carbon nitride, which could be stable in the visible region and have good photocatalytic ability to decompose water to generate hydrogen. After 10 hours of illumination, the hydrogen production was 5449.5 umol/g, it was 50.8 times of the hydrogen production of graphene/g-C_3N_4 composite under consistent experimental conditions, and the composite exhibited enduring stability. High photocatalytic performance was due to the combination of fullerenes and graphene, and a large amount of electrons were generated in the composite catalyst, which strengthened the utilization of photogenerated electrons and increased the catalytic effect, thereby improving the photocatalytic efficiency. Guan et al. [73] used a solid-state mechanochemical route to produce MoS_2-C_{60} hybrid with a van der Waals heterostructure (Fig. 19A). The C_{60} cluster protective layer formed in the skeleton improves the light absorbing ability on the one hand, and greatly accelerated electrons transfer to the surface of the C_{60} cluster on the other hand. Supported C_{60} clusters can also be used as electron transport stations for rapid electron capture from the composite catalyst; and it also could be used as H_2 precipitation active site to absorb and reduce H^+, thereby promoting the precipitation of H_2 (Fig. 19B). When the composite catalyst contained

2.8% C_{60}, it exhibited the best hydrogen production efficiency, and the highest H_2 production rate reached 6.89 mmol $h^{-1}g^{-1}$ (Fig. 19C). Song et al. [138] prepared $Cr_{2-x}Fe_xO_3$ nanoparticles first, and then prepared $C_{60}/Cr_{2-x}Fe_xO_3$ composites (Fig. 20). The results showed that the prepared C_{60}-$Cr_{2-x}Fe_xO_3$ nanocomposite exhibited excellent activity for hydrogen production without any precious metal under visible light irradiation. Research showed that 3% C_{60}-$Cr_{1.3}Fe_{0.7}O_3$ composite catalyst exhibits the best performance (220.5 μmol $h^{-1}g^{-1}$) (Fig. 20C). The results showed that the catalyst had good hydrogen production performance under weak alkaline conditions.

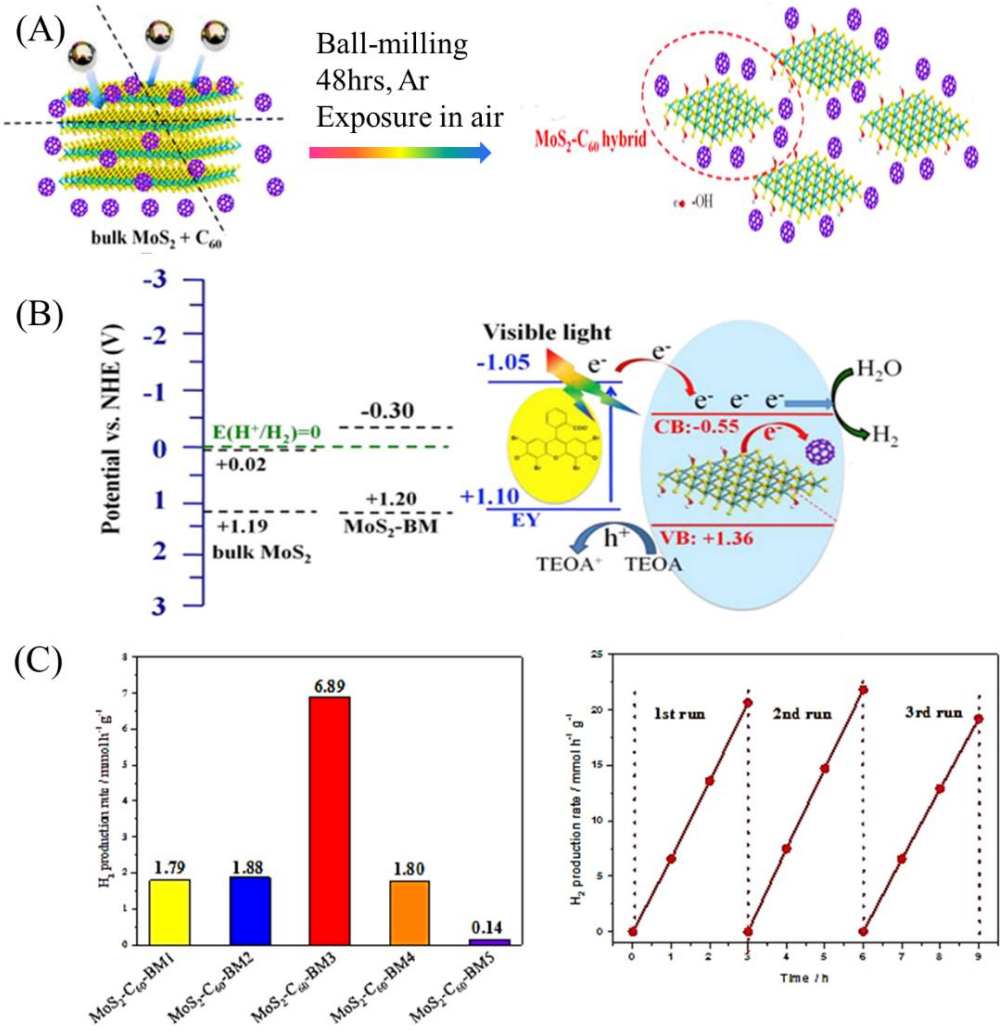

Fig. 19.(A) Schematic diagram of mechanochemical reaction between MoS_2 and C_{60}; (B) hydrogen production mechanism and electron transfer process of MoS_2-C_{60} photocatalyst under visible light; (C) Photocatalytic H_2 production rates of various materials and typical time courses of H_2 production based on MoS_2-C_{60}-BM3 (MoS_2 ball-milled without C_{60}) [73]. Copyright 2018 Elsevier.

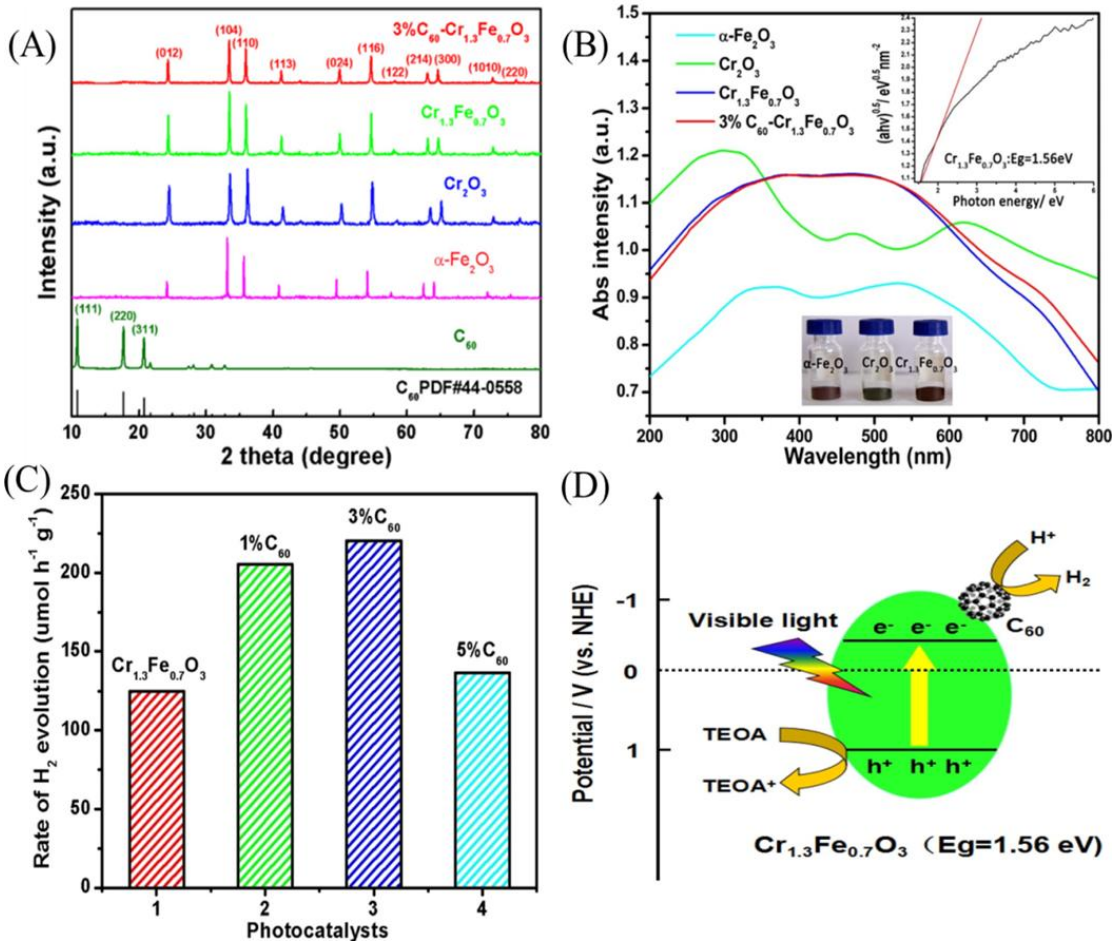

Fig. 20.(A) XRD patters of C60, a-Fe_2O_3,Cr_2O_3,$Cr_{1.3}Fe_{0.7}O_3$ and 3%C_{60}–$Cr_{1.3}Fe_{0.7}O_3$; (B) UV–vis-diffuse reflectance spectra of bare a-Fe_2O_3,Cr_2O_3,$Cr_{1.3}Fe_{0.7}O_3$ and 3% C_{60}–$Cr_{1.3}Fe_{0.7}O_3$; (C) Photocatalytic H_2 evolution rates of $Cr_{1.3}Fe_{0.7}O_3$ and C_{60}–$Cr_{1.3}Fe_{0.7}O_3$ with different C_{60} contents under visible light irradiation with triethanolamine as a hole scavenger; (D) A possible mechanism for the improve migration efficiency of photogenerated electron on the photocatalyst

interface for the 3%C_{60}-$Cr_{1.3}Fe_{0.7}O_3$ composite system [138]. Copyright 2015 Elsevier.

To propose a deep insight (the role of nitrogen) into understanding the improved photocatalytic ability of the C_{60}/g-C_3N_4 nanocomposites, Li et al. [188] constructed C_{60}/g-C_3N_4 hybrid models in which C_{60} is at the N_1, N_3 and I_2 sites above the g-C_3N_4 monolayer. As can be seen from the adhesive energy, the most advantageous adhesion site was I_2 (Figs. 21A,B), and then enhanced light absorption (Fig. 21C) and contributed to efficient charge separation. Finally, the traditional type II heterojunction mechanism was proposed to explain the charge transfer pathway (Fig. 21D).

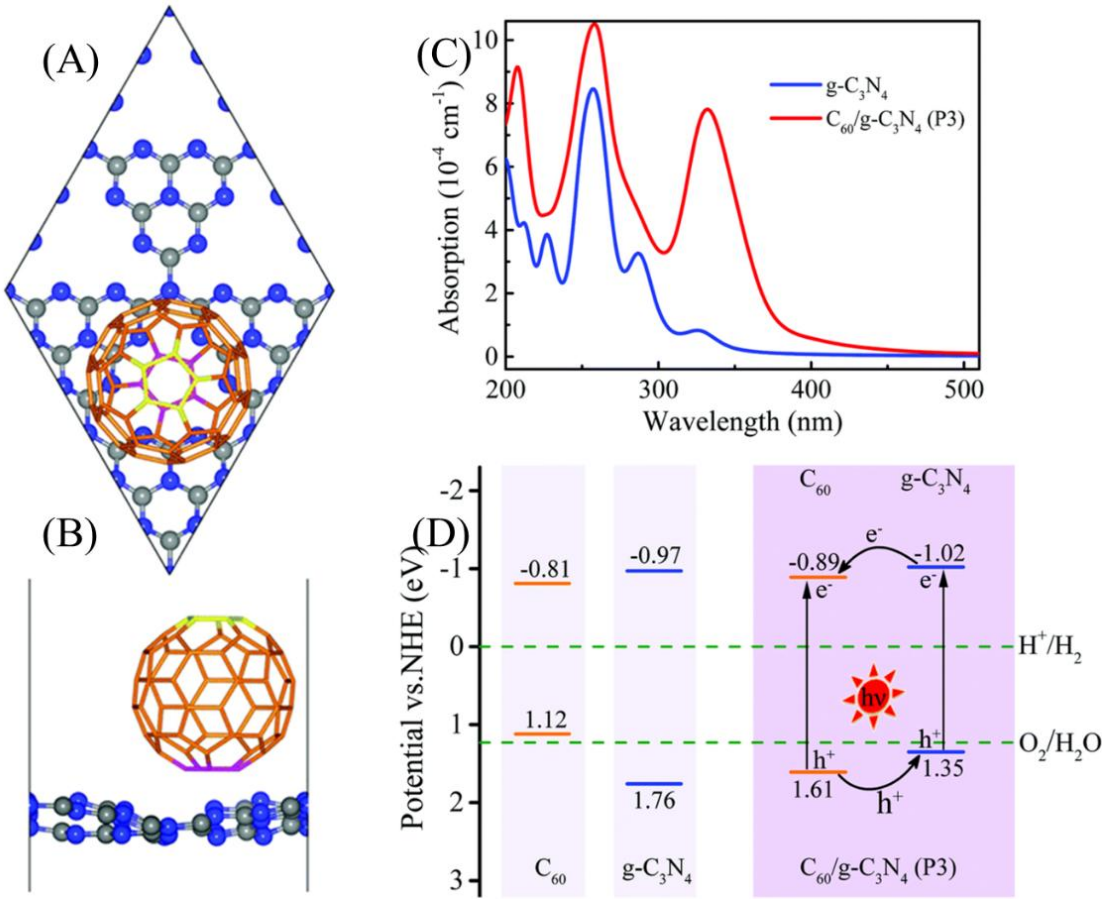

Fig. 21. (A) Top view and (B) side view of optimized C_{60}/g-C_3N_4 model. (C) Optical absorption

spectra of g-C_3N_4 and C_{60}/g-C_3N_4. (D) Proposed charge transfer route between C_{60} and g-C_3N_4 [188]. Copyright 2016 Royal Society of Chemistry.

All of the above are photocatalysts composed of a combination of fullerenes and inorganic materials. In recent years, research on organic material photocatalysts has attracted people's attention, and there has been more and more attention in the compounding of fullerenes and organic materials. Abe et al. [68] prepared a new advanced Pt-loaded H_2Pc/C_{60} p-n heterojunction composite photocatalyst that promoted hydrogen generation over the entire visible range. The effects of the incident light intensity, the double layer film thickness of the catalyst and the deposition amount of Pt on the hydrogen production performance were investigated. The research team [69] also prepared fullerene C_{60}/ZnPc composite photocatalyst. It was a p-n heterojunction organic photocatalyst for the decomposition of hydrazine (N_2H_4) while using H^+ to generate hydrogen over entire visible range. Huo et al. prepared a new type of cost-effective fullerene organic photocatalyst. It was used as a photoluminescent agent and a photocatalyst to produce hydrogen, had a higher activity (7.39 mmol $h^{-1}g^{-1}$) than a single compound [189].

1319 Table.3 Fullerene modified photocatalysts for hydrogen production.

Photocatalyst	Preparation method	Fullerene content [wt%]	Incident light	Light intensity	Cocatalyst	Activity	Quantum efficiency	Increased multiple	Ref
C_{60}/graphene/g-C_3N_4	hydrothermal	-	λ > 420 nm	5 W light-emitting diode	Pt	545 μmol $h^{-1}g^{-1}$	7.2%	50.8	[164]
C_{60}/CdS/TiO_2	ionexchanged	0.5	λ = 420 nm	3 W UV-LEDs	-	6.03 mmol $h^{-1}g^{-1}$	2.0%	8.5	[139]
C_{60}/$Cr_{2-x}Fe_xO_3$	absorption	3	λ > 420 nm	300W Xe lamp	-	220.5 μmol $h^{-1}g^{-1}$	-	1.77	[138]
C_{60}/bithiazole–Ru	solvothermal	2	Visible light	300 W Xe arc lamp	Ru	7.39 mmol $h^{-1}g^{-1}$	4.27%	5	[189]
C_{60}-dCNTs/TiO_2	hydrothermal	5	UV light	300 W Xe-lamp	-	651 μmol $h^{-1}g^{-1}$	-	10	[190]
C_{60}-MoS_2	mechanochemical	2.8	Visible light	300 W Xe-lamp	-	6.89 mmol $h^{-1}g^{-1}$	6.4%	9.5	[73]
C_{60}/ZnPc	vapour deposition	-	λ < 750 nm	-	Pt	-	-	-	[69]
WO_3@C_{60}	hydrothermal	4	λ > 420 nm	300 W Xe-lamp	-	150 mmol $h^{-1}g^{-1}$	-	1.88	[165]

5. Conclusions and outlook

Due to the unique structure and physical properties of fullerenes, when fullerene C_{60} and its derivatives combined with semiconductor materials, fullerene C_{60} affects the electron transfer process and composite materials. On one hand, in the photocatalytic electron transport process, C_{60} mainly accelerates the photocatalytic reaction process by four modes of action: electron acceptor, electron donor, energy transfer mediator, electron donor and acceptor. On the other hand, C_{60} and its derivatives can regulate the crystal growth, prevent material deactivation and adjust the band gap in the composite materials to enhance the catalytic performance of the composite. Therefore, the properties of fullerenes/semiconductor composites are obviously enhanced, which is conducive to further expanding the application range of semiconductor materials.

As for the mechanism of photocatalytic enhancement of composite materials, there is a consensus in the current literature that there is a synergetic effect between fullerenes and semiconductor materials, that is, the composite can enhance their photocatalytic efficiency and adsorption performance, and the optimal content of fullerenes in composite materials is not the more the better. However, at present, various reaction principles of photocatalytic efficiency enhancement, especially the visible light catalysis mechanism, is still not deep enough. In addition, there are still

many problems and challenges here, and we need further research and exploration,which is outlined in Figure 22.

(1) More efforts are needed to better understand fullerene/ semiconductor photocatalysts for practical requirements, such as examining the photocatalytic selectivity in a solution containing more components, the chemical stability of these catalysts under different pH and temperature conditions during the experiments, etc. Besides, some scholars have done some quantitative researches on the effects of factors such as the thickness and size of C_{60} and its derivatives on the performance of composite systems. However, the qualitative researches on the influence of the surface composition of composite catalysts prepared by different precursors and methods on the interaction of semiconductor nanomaterials are still relatively rare.

(2) Fullerene and its derivatives are relatively expensive and difficult to prepare, to our knowledge, the key to determining the fullerene price and its practical application is the purification of fullerenes. We mainly need to develop new fullerene purification technology to reduce the difficulty of this process. More importantly, fullerene C_{60} and its derivatives are only trace amounts in photocatalytic applications. In some simple applications, fullerene C_{60} with lower purity can also be put into use, which facilitates our mass production and use. With the deepening of research and the development of preparation technology, accurate quantitative research will be reached, and eventually will get a wide range of applications.

(3) The simulation of properties of fullerene-semiconductor composites by theoretical calculation method is helpful to reveal the photocatalytic mechanism and optimize the composition and structure of fullerene-semiconductor composites, which can improve the photoquantum efficiency. Therefore, theoretical calculations provide a huge role for our researchers in studying high-activity photocatalysts, designing new photocatalytic cracking agents, changing internal properties and microstructure of fullerene-based composites, and designing the electronic structure of active surfaces on the basis of describing photocatalytic reactions. In future research, we should pay attention to the combination of experiments and theoretical calculations to better reflect the internal reaction mechanism.

(4) The structure of the heterojunction is of great help to increase photocatalytic activity of materials. Nevertheless, there are still relatively few studies on these aspects. Therefore, there is still much room for exploration in the configuration control of fullerene modified composite catalysts. In order to obtain better configurations such as surface dispersion, semiconductor nanomaterials can be controlled into easily dispersed zero-dimensional crystals or quantum dots, or they can be controlled into one-dimensional materials that can rapidly conduct electrons, such as nanotubes, nanorods and nanowires, and then composite with fullerenes. Most of the research in this area of research is still at the laboratory scale stage and only a small amount of catalyst has been synthesized. Moreover, some of these synthetic methods are very complex and difficult to control. Therefore, it is highly

desirable to develop a simpler synthesis method (especially the one-step synthesis methods) that can be used for mass production.

(5) Research on fullerenes and their derivatives should be further advanced. On the one hand, the previous fullerene materials were mainly C60, but the fullerene family is a huge system, and there are many types that we have not yet applied to environmental catalysis. On the other hand, fullerene derivatives are mainly modified by some organic groups and metal groups, such as amino and hydroxyl groups. In order to obtain better performance derivatives, it should try to improve conditions and methods to obtain derivatives with special properties to meet the needs of practical applications. There is still relatively little research work in this area, and it is worth trying to find out.

(6) The treatment of pollutants in water is mainly focused on the treatment of organic dyes and heavy metal ions. More attention should be paid to the persistent organic pollutants that need to be treated, such as antibiotic pollutants. In the field of environmental remediation except the treatment of water pollution, there is also the treatment of gas phase pollutants, such as the reduction of nitrogen oxides and greenhouse gases. In addition to the generation of hydrogen, it can also be applied to other energy synthesis in the energy field. Besides, the environmental risk assessment of these nanostructure photocatalysts should be adequately conducted before practical applications. Particularly, for the pollutants degradation applications, the toxicity of intermediate products needs to be carefully evaluated since

photocatalytic degradation often fails to completely mineralize the pollutants.

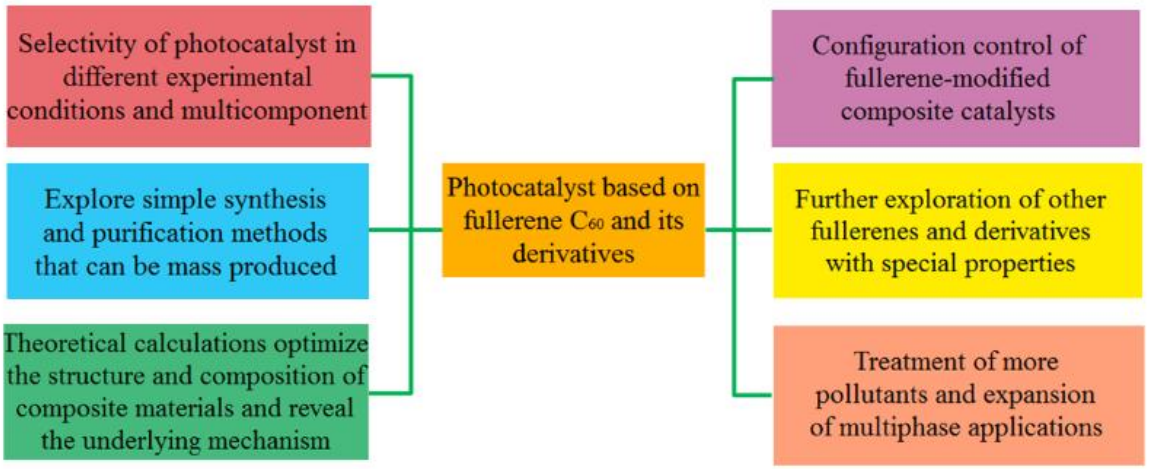

Fig.22. Future challenges and research directions for fullerene C_{60} photocatalysis.

Abbreviation

APTES	Aminopropyl triethoxysilane
BPA	Bisphenol A
BET	Brunauer−Emmett−Teller
CB	Conduction band
CNTs	Carbon nanotubes
CQDs	Carbon quantum dots
CTAB	Cetyltrimethylammonium bromide
DOS	Density of state
EDS	Energy dispersive spectrometer
FTIR	Fourier transform infrared spectrum

1416	FESEM	Field emission scanning electron microscope
1417	HRTEM	High resolution transmission electron microscope
1418	HOL	Highest-occupied levels
1419	ISC	Intersystem crossing
1420	MB	Methylene biue
1421	MO	Methylene orange
1422	MCPBA	M-Chloroperbenzoic acid
1423	LUL	Lowest-unoccupied level
1424	PL	Photoluminescence
1425	ROS	Reactive oxygen species
1426	SEM	Scanning electron microscope
1427	TEOS	Tetraethoxysilane
1428	TiNTs	Titania nanotubes
1429	TEM	Transmission electron microscopy
1430	TPSA	Triethoxysilyl propylsuccinic anhydride
1431	UV	Ultraviolet
1432	UV–vis DRS	UV–vis diffuse-reflectance spectra
1433	VB	Valence band
1434	XRD	X-ray diffraction
1435	XPS	X-ray photoelectron spectroscopy
1436	ZnAlTi-LDO	ZnAlTi layered double oxide

Acknowledgements

The study was financially supported by the Program for Changjiang Scholars and Innovative Research Team in University (IRT-13R17), the National Natural Science Foundation of China (51679085, 51378192, 51039001, 51378190, 51521006, 51508177), the Fundamental Research Funds for the Central Universities of China (531118010055), the Funds of Hunan Science and Technology Innovation Project (2018RS3115).

References

[1] Y. Pan, X. Yuan, L. Jiang, H. Yu, J. Zhang, H. Wang, R. Guan, G. Zeng, Recent advances in synthesis, modification and photocatalytic applications of micro/nano-structured zinc indium sulfide, Chem. Eng. J. 354 (2018) 407-431.

[2] B. Shao, Z. Liu, H. Zhong, G. Zeng, G. Liu, M. Yu, Y. Liu, X. Yang, Z. Li, Z. Fang, J. Zhang, C. Zhao, Effects of rhamnolipids on microorganism characteristics and applications in composting: A review, Microbiol. Res. 200 (2017) 33-44.

[3] M. Liu, J. Xu, B. Cheng, W. Ho, J. Yu, Synthesis and adsorption performance of $Mg(OH)_2$ hexagonal nanosheet–graphene oxide composites, Appl. Surf. Sci. 332 (2015) 121-129.

[4] Q. Liang, X. Liu, G. Zeng, Z. Liu, L. Tang , B. Shao, Z. Zeng, W. Zhang, Y. Liu, M. Cheng, W. Tang, S. Gong, Surfactant-assisted synthesis of photocatalysts: Mechanism, synthesis, recent advances and environmental application, Chem. Eng. J. 372 (2019) 429-451.

[5] A. Fujishima, K. Honda, Electrochemical photolysis of water at a semiconductor electrode, Nature 238 (1972) 37-38.

[6] Y. Liu, Z. Liu, D. Huang, M. Cheng, G. Zeng, C. Lai, C. Zhang, C. Zhou, W. Wang, D. Jiang, H. Wang, B. Shao, Metal or metal-containing nanoparticle@MOF nanocomposites as a promising type of photocatalyst., Coord. Chem. Rev. 388 (2019) 63-78.

[7] M. Yu, Z. Liu, G. Zeng, H. Zhong, Y. Liu, Y. Jiang, M. Li, X. He, Y. He, Characteristics of mannosylerythritol lipids and their environmental potential, Carbohydr. Res. 407 (2015) 63-72.

[8] S. Kumar, A. K. Ojha, D. Patrice, B. S. Yadav, A. Materny, One-step in situ synthesis of CeO_2 nanoparticles grown on reduced graphene oxide as an excellent fluorescent and photocatalyst material under sunlight irradiation, Phys. Chem. Chem. Phys. 18 (2016) 11157-11167.

[9] S. Kumar, A. K. Ojha, Ni, Co and Ni–Co codoping induced modification in shape, optical band gap and enhanced photocatalytic activity of CeO_2 nanostructures for photodegradation of methylene blue dye under visible light irradiation, RSC Adv. 6 (2016) 8651-8660.

[10] L. Jiang, X. Yuan, Y. Pan, J. Liang, G. Zeng, Z. Wu, H. Wang, Doping of graphitic carbon nitride for photocatalysis: A reveiw, Appl. Catal. B Environ. 217 (2017) 388-406.

[11] W. Jones, D. J. Martin, A. Caravaca, A. M. Beale, M. Bowker, T. Maschmeyer, G. Hartley, A. Masters, A comparison of photocatalytic reforming reactions of methanol and triethanolamine with Pd supported on titania and graphitic carbon nitride, Appl. Catal. B Environ. 240 (2019) 373-379.

[12] Y. Tan, Z. Shu, J. Zhou, T. Li, W. Wang, Z. Zhao, One-step synthesis of nanostructured g-C_3N_4/TiO_2 composite for highly enhanced visible-light photocatalytic H_2 evolution, Appl. Catal. B Environ. 230 (2018) 260-268.

[13] S. G. Ullattil, S. B. Narendranath, S. C. Pillai, P. Periyat, Black TiO_2 Nanomaterials: A Review of Recent Advances, Chem. Eng. J. 343 (2018) 708-736.

[14] H. Yi, D. Huang, L. Qin, G. Zeng, C. Lai, M. Cheng, S. Ye, B. Song, X. Ren, X. Guo,

Selective prepared carbon nanomaterials for advanced photocatalytic application in environmental pollutant treatment and hydrogen production, Appl. Catal. B Environ. 239 (2018) 408-424.
[15] T. Wu , X. Liu, Y. Liu , M. Cheng , Z. Liu , G. Zeng , B. Shao, Q. Liang , W. Zhang , Q. He , W. Zhang Application of QD-MOF composites for photocatalysis: Energy production and environmental remediation, Coord. Chem. Rev. 403 (2020) 213097.
[16] H. Wang, X. Yuan, Y. Wu, G. Zeng, H. Dong, X. Chen, L. Leng, Z. Wu, L. Peng, In situ synthesis of In_2S_3@MIL-125(Ti) core-shell microparticle for the removal of tetracycline from wastewater by integrated adsorption and visible-light-driven photocatalysis, Appl. Catal. B Environ. 186 (2016) 19-29.
[17] R. Asahi, T. Morikawa, T. Ohwaki, K. Aoki, Y. Taga, Visible-light photocatalysis in nitrogen-doped titanium oxides, Science 293 (2001) 269-271.
[18] H. Wang, X. Yuan, Y. Wu, X. Chen, L. Leng, G. Zeng, Photodeposition of metal sulfides on titanium metal-organic frameworks for excellent visible-light-driven photocatalytic Cr(VI) reduction, RSC Adv. 5 (2015) 32531-32535.
[19] H. Jiang, J. Liu, K. Cheng, W. Sun, J. Lin, Enhanced Visible Light Photocatalysis of Bi_2O_3 upon Fluorination, J. Phys. Chem. C 117 (2013) 20029-20036.
[20] L. Zhou, W. Wang, H. Xu, S. Sun, M. Shang, Bi_2O_3 Hierarchical Nanostructures: Controllable Synthesis, Growth Mechanism, and their Application in Photocatalysis, Chem.-Eur. J. 15 (2009) 1776-1782.
[21] B. Shao, Z. Liu, G. Zeng, Z. Wu, Y. Liu, M. Cheng, M. Chen, Y. Liu, W. Zhang, H. Feng, Nitrogen-Doped Hollow Mesoporous Carbon Spheres Modified g-C_3N_4/Bi_2O_3 Direct Dual Semiconductor Photocatalytic System with Enhanced Antibiotics Degradation under Visible Light, ACS Sustain. Chem. Eng. 6 (2018) 16424-16436.
[22] S. K. Mohapatra, S. E. John, S. Banerjee, M. Misra, Water Photooxidation by Smooth and Ultrathin alpha-Fe_2O_3 Nanotube Arrays, Chem. Mater. 21 (2009) 3048-3055.
[23] J. Zhu, Z. Yin, D. Yang, T. Sun, H. Yu, H. E. Hoster, H. H. Hng, H. Zhang, Q. Yan, Hierarchical hollow spheres composed of ultrathin Fe_2O_3 nanosheets for lithium storage and photocatalytic water oxidation, Energy Environ. Sci. 6 (2013) 987-993.
[24] G. R. Bamwenda, H. Arakawa, The visible light induced photocatalytic activity of tungsten trioxide powders, Appl. Catal. A General 210 (2001) 181-191.
[25] W. Zeng, T. Cai, Liu.Yutang, L. Wang, W. Dong, H. Chen, X. Xia, An artificial organic-inorganic Z-scheme photocatalyst WO_3@Cu@PDI supramolecular with excellent visible light absorption and photocatalytic activity, Chem. Eng. J. 381 (2019) 122691.
[26] J. Xu, L. Li, C. Guo, Y. Zhang, W. Meng, Photocatalytic degradation of carbamazepine by tailored $BiPO_4$: efficiency, intermediates and pathway, Appl. Catal. B Environ. 130 (2013) 285-292.
[27] J. Wang, J. Li, H. Li, S. Duan, S. Meng, X. Fu, S. Chen, Crystal phase-controlled synthesis of $BiPO_4$ and the effect of phase structure on the photocatalytic degradation of gaseous benzene, Chem. Eng. J. 330 (2017) 433-441.
[28] Y. Zhang, J. Yu, D. Yu, X. Zhou, W. Lu, Enhancement in the photocatalytic and

photoelectrochemical properties of visible-light driven $BiVO_4$ photocatalyst, Rare Metals 30 (2011) 192-198.
[29] R. Venkatesan, S. Velumani, K. Ordon, M. Makowska-Janusik, G. Corbel, A. Kassiba, Nanostructured bismuth vanadate ($BiVO_4$) thin films for efficient visible light photocatalysis, Mater. Chem. Phys. 205 (2018) 325-333.
[30] J. Ma, J. Zou, L. Li, C. Yao, T. Zhang, D. Li, Synthesis and characterization of Ag_3PO_4 immobilized in bentonite for the sunlight-driven degradation of Orange II, Appl. Catal. B Environ. 134 (2013) 1-6.
[31] D. J. Martin, G. Liu, S. J. A. Moniz, Y. Bi, A. M. Beale, J. Ye, J. Tang, Efficient visible driven photocatalyst, silver phosphate: performance, understanding and perspective, Chem. Soc. Rev. 44 (2015) 7808-7828.
[32] B. Shao , X. Liu, Z. Liu, G. Zeng, Q. Liang, C. Liang, Y. Cheng, W. Zhang, Y. Liu, S. Gong, A novel double Z-scheme photocatalyst $Ag_3PO_4/Bi_2S_3/Bi_2O_3$ with enhanced visible-light photocatalytic performance for antibiotic degradation, Chem. Eng. J. 368 (2019) 730-745.
[33] H. B. Fu, C. S. Pan, W. Q. Yao, Y. F. Zhu, Visible-light-induced degradation of rhodamine B by nanosized Bi_2WO_6, J. Phys. Chem. B 109 (2005) 22432-22439.
[34] J. W. Tang, Z. G. Zou, J. H. Ye, Photocatalytic decomposition of organic contaminants by Bi_2WO_6 under visible light irradiation, Catal. Lett. 92 (2004) 53-56.
[35] L. Zhang, W. Wang, L. Zhou, H. Xu, Bi_2WO_6 nano- and microstructures: Shape control and associated visible-light-driven photocatalytic activities, Small 3 (2007) 1618-1625.
[36] J. Chen, X. Wu, L. Yin, B. Li, X. Hong, Z. Fan, B. Chen, C. Xue, H. Zhang, One-pot Synthesis of CdS Nanocrystals Hybridized with Single-Layer Transition-Metal Dichalcogenide Nanosheets for Efficient Photocatalytic Hydrogen Evolution, Angew. Chem. Int. Ed. 54 (2015) 1210-1214.
[37] Y. Wu, H. Wang, W. Tu, S. Wu, Y. Liu, Y. Tan, H. Luo, X. Yuan, W. C. Jia, Petal-like CdS nanostructures coated with exfoliated sulfur-doped carbon nitride via chemically activated chain termination for enhanced visible-light–driven photocatalytic water purification and H_2 generation, Appl. Catal. B Environ. 229 (2018) 181-191.
[38] B. Shao, X. Liu, Z. Liu, G. Zeng, W. Zhang, Q. Liang, Y. Liu, Q. He, X. Yuan, D. Wang, S. Luo, S. Gong, Synthesis and characterization of 2D/0D g-C_3N_4/CdS-nitrogen doped hollow carbon spheres (NHCs) composites with enhanced visible light photodegradation activity for antibiotic, Chem. Eng. J. 374 (2019) 479–493.
[39] H. Wang, X. Yuan, Y. Wu, G. Zeng, X. Chen, L. Leng, H. Li, Synthesis and applications of novel graphitic carbon nitride/metal-organic frameworks mesoporous photocatalyst for dyes removal, Appl. Catal. B Environ. 174-175 (2015) 445-454.
[40] W. Zhang, J. Zhang, F. Dong, Y. Zhang, Facile synthesis of in-situ phosphorus-doped g-C_3N_4 with enhanced visible light photocatalytic NO purification, RSC Adv. 6 (2016) 88085-88089.
[41] S. Hu, L. Ma, J. You, F. Li, Fan, Z. Fan, F. Wang, D. Liu, J. Gui, A simple and efficient method to prepare a phosphorus modified g-C_3N_4 visible light photocatalyst, RSC Adv. 4 (2014) 21657-21663.

[42] W. Kratschmer, L. D. Lamb, K. Fostiropoulos, D. R. Huffman, Solid C_{60}: a new form of carbon, Nature 347 (1990) 354-357.
[43] Z. Peng, X. Liu, W. Zhang, Z. Zeng, Z. Liu, C. Zhang, Y. Liu, B. Shao, Q. Liang, W. Tang, X. Yuan, Advances in the application, toxicity and degradation of carbon nanomaterials in environment: A review, Environ. Int. 134 (2020) 105298.
[44] G. Black, M. a. T. Black, D. Solan, D. Shropshire, Carbon free energy development and the role of small modular reactors: A review and decision framework for deployment in developing countries, Renew. Sust. Energ. Rev. 43 (2015) 83-94.
[45] S. Faraji, F. N. Ani, The development supercapacitor from activated carbon by electroless plating—A review, Renew. Sust. Energ. Rev. 42 (2015) 823-834.
[46] H. Sun, J. Deng, L. Qiu, X. Fang, H. Peng, Recent progress in solar cells based on one-dimensional nanomaterials, Energy Environ. Sci. 8 (2015) 1139-1159.
[47] H. Zhong, C. H. Wu, C. Z. Li, J. Carpenter, C. C. Chueh, J. Y. Chen, H. Ade, A. K. Jen, Rigidifying Nonplanar Perylene Diimides by Ring Fusion Toward Geometry-Tunable Acceptors for High-Performance Fullerene-Free Solar Cells, Adv. Mater. 28 (2016) 951-958.
[48] B. Shao, Z. Liu, G. Zeng, Y. Liu, X. Yang, C. Zhou, M. Chen, Y. Liu, Y. Jiang, M. Yan, Immobilization of laccase on hollow mesoporous carbon nanospheres: Noteworthy immobilization, excellent stability and efficacious for antibiotic contaminants removal, J. Hazard. Mater. 362 (2019) 318-326.
[49] G. K. Pradhan, D. K. Padhi, K. M. Parida, Fabrication of alpha-Fe_2O_3 Nanorod/RGO Composite: A Novel Hybrid Photocatalyst for Phenol Degradation, ACS Appl. Mater. Interfaces 5 (2013) 9101-9110.
[50] R. C. Pawar, S. Kang, S. H. Ahn, C. S. Lee, Gold nanoparticle modified graphitic carbon nitride/multi-walled carbon nanotube (g-C_3N_4/CNTs/Au) hybrid photocatalysts for effective water splitting and degradation, RSC Adv. 5 (2015) 24281-24292.
[51] X. Xiao, W. Zhang, Photocatalysis of Carbon Nanotubes/Semiconductor Composites, Prog. Chem. 23 (2011) 657-668.
[52] Q. Cao, Q. Yu, D. W. Connell, G. Yu, Titania/carbon nanotube composite (TiO_2/CNT) and its application for removal of organic pollutants, Clean Technol. Environ. Policy 15 (2013) 871-880.
[53] R. Leary, A. Westwood, Carbonaceous nanomaterials for the enhancement of TiO_2 photocatalysis, Carbon 49 (2011) 741-772.
[54] X. Huang, X. Qi, F. Boey, H. Zhang, Graphene-based composites, Chem. Soc. Rev. 41 (2012) 666-686.
[55] N. Zhang, Y. Zhang, Y. Xu, Recent progress on graphene-based photocatalysts: current status and future perspectives, Nanoscale 4 (2012) 5792-5813.
[56] H. Tang, C. M. Hessel, J. Y. Wang, N. Yang, R. Yu, H. Zhao, D. Wang, Two-dimensional carbon leading to new photoconversion processes, Chem. Soc. Rev. 43 (2014) 4281-4299.
[57] Y. Zhao, H. Tang, N. Yang, D. Wang, Graphdiyne: Recent Achievements in Photo- and Electrochemical Conversion, Adv.Sci. 5 (2018) 1800959.
[58] S. Sepahvand, S. Farhadi, Fullerene-modified magnetic silver phosphate

($Ag_3PO_4/Fe_3O_4/C_{60}$) nanocomposites: hydrothermal synthesis, characterization and study of photocatalytic, catalytic and antibacterial activities, RSC Adv. 8 (2018) 10124-10140.
[59] O. Ito, F. D'souza, Recent advances in photoinduced electron transfer processes of fullerene-based molecular assemblies and nanocomposites, Molecules 17 (2012) 5816-5835.
[60] H. Imahori, Y. Sakata, Donor-linked fullerenes: photoinduced electron transfer and its potential application, Adv. Mater. 9 (1997) 537-546.
[61] K. Toshifumi, F. Mamoru, I. Osamu , T. Yasumasa , Y. Usui, C_{60} as Photosensitizing Electron-Transfer Mediator for Ion-Pair Charge-Transfer Complexes between Borate Anions and Methyl Viologen Dication, J. Phys. Chem. A 103 (1999) 9938-9942.
[62] H. Fu, T. Xu, S. Zhu, Y. Zhu, Photocorrosion inhibition and enhancement of photocatalytic activity for ZnO via hybridization with C_{60}, Environ. Sci. Technol. 42 (2008) 8064-8069.
[63] M. Pawel, G. P. Tegos, G. Hariprasad, W. Tim, S. Tadeusz, M. R. Hamblin, Photodynamic therapy with fullerenes, Photoch. Photobio.Sci. 6 (2007) 1139-1149.
[64] Y. Zhong, R. Munir, A. H. Balawi, A. D. Sheikh, L. Yu, M. Tang, H. Hu, F. Laquai, A. Amassian, Mesostructured Fullerene Electrodes for Highly Efficient n-i-p Perovskite Solar Cells, ACS Energy Lett. 1 (2016) 1049-1056.
[65] J. Ge, Y. Zhang, S.-J. Park, Recent Advances in Carbonaceous Photocatalysts with Enhanced Photocatalytic Performances: A Mini Review, Materials 12 (2019) 1916.
[66] W. Bai, V. Krishna, J. Wang, B. Moudgil, B. Koopman, Enhancement of nano titanium dioxide photocatalysis in transparent coatings by polyhydroxy fullerene, Appl. Catal. B Environ. 125 (2012) 128-135.
[67] A. Djordjevic, D. Sojic Merkulov, M. Lazarevic, I. Borisev, I. Medic, V. Pavlovic, B. Miljevic, B. Abramovic, Enhancement of nano titanium dioxide coatings by fullerene and polyhydroxy fullerene in the photocatalytic degradation of the herbicide mesotrione, Chemosphere 196 (2018) 145-152.
[68] T. Abe, J. Chiba, M. Ishidoya, K. Nagai, Organophotocatalysis system of p/n bilayers for wide visible-light-induced molecular hydrogen evolution, RSC Adv. 2 (2012) 7992-7996.
[69] T. Abe, N. Taira, Y. Tanno, Y. Kikuchi, K. Nagai, Decomposition of hydrazine by an organic fullerene-phthalocyanine p-n bilayer photocatalysis system over the entire visible-light region, Chem Commun (Camb) 50 (2014) 1950-1952.
[70] P. Arunachalam, S. Zhang, T. Abe, M. Komura, T. Iyoda, K. Nagai, Weak visible light (～ mW/cm^2) organophotocatalysis for mineralization of amine, thiol and aldehyde by biphasic cobalt phthalocyanine/fullerene nanocomposites prepared by wet process, Appl. Catal. B Environ. 193 (2016) 240-247.
[71] L. Huang, J. Zhao, C_{60}-Bodipy dyad triplet photosensitizers as organic photocatalysts for photocatalytic tandem oxidation/[3+2] cycloaddition reactions to prepare pyrrolo[2,1-a]isoquinoline, Chem Commun (Camb) 49 (2013) 3751-3753.
[72] X. Bai, L. Wang, Y. Wang, W. Yao, Y. Zhu, Enhanced oxidation ability of g-C_3N_4 photocatalyst via C_{60} modification, Appl. Catal. B Environ. 152-153 (2014) 262-270.
[73] J. Guan, J. H. Wu, D. C. Jiang, X. J. Zhu, R. N. Guan, X. Y. Lei, P. W. Du, H. L. Zeng, S. F. Yang, Hybridizing MoS_2 and C_{60} via a van der Waals heterostructure toward synergistically

enhanced visible light photocatalytic hydrogen production activity, Int. J. Hydrogen Energy 43 (2018) 8698-8706.
[74] K. J. Moor, D. C. Valle, L. Chuanhao, K. Jae Hong, Improving the Visible Light Photoactivity of Supported Fullerene Photocatalysts through the Use of [C_{70}] Fullerene, Environ. Sci. Technol. 49 (2015) 6190-6197.
[75] E. Osawa, Superaromaticity, Kagaku 25 (1970) 854-863.
[76] C. S. Yannoni, R. D. Johnson, G. Meijer, D. S. Bethune, J. R. Salem, 13C NMR study of the C_{60} cluster in the solid state: molecular motion and carbon chemical shift anisotropy, J. Phys. Chem. 95 (1991) 9-10.
[77] H. W. Kroto, J. R. Heath, S. C. O'brien, R. F. Curl, R. E. Smalley, C_{60}: Buckminsterfullerene, Nature 318 (1985) 162-163.
[78] R. Tycko, R. C. Haddon, G. Dabbagh, S. H. Glarum, D. C. Douglass, A. M. Mujsce, Solid-state magnetic resonance spectroscopy of fullerenes, J. Phys. Chem. 95 (1991) 518-520.
[79] Q. M. Zhang, J. Yi, J. Bernholc, Structure and dynamics of solid C_{60}, Phys. Rev. Lett. 66 (1991) 2633-2636.
[80] S. Saito, A. Oshiyama, Cohesive mechanism and energy bands of solid C_{60}, Phys.rev.lett 66 (1991) 2637-2640.
[81] Y. Quo, N. Karasawa, W. a. G. Iii, Prediction of fullerene packing in C_{60} and C_{70} crystals, Nature 351 (1991) 464-467.
[82] M. A. Verheijen, H. Meekes, G. Meijer, E. Raas, P. Bennema, Growth and morphology of C_{60} crystals, Chem. Phys. Lett. 191 (1992) 339-344.
[83] M. Chen, G. Zhang, Y. Jiang, K. Yin, L. Zhang, H. Li, J. Hao, Fullerene-Directed Synthesis of Flowerlike $Cu_3(PO_4)_2$ Crystals for Efficient Photocatalytic Degradation of Dyes, Langmuir 35 (2019) 8806-8815.
[84] R. Gao, Q. Dai, F. Du, D. Yan, L. Dai, C-60-Adsorbed Single-Walled Carbon Nanotubes as Metal-Free, pH-Universal, and Multifunctional Catalysts for Oxygen Reduction, Oxygen Evolution, and Hydrogen Evolution, J. Am. Chem. Soc. 141 (2019) 11658-11666.
[85] J. W. Ko, W. B. Ko, Preparation of C_{60} fullerene nanowhisker-cadmium sulfide nanoparticle composite and its photocatalytic activity for degradation of rhodamine B, Fuller. Nanotub. Carbon Nanostruct. 27 (2019) 895-898.
[86] V. Martinez-Agramunt, E. Peris, Photocatalytic Properties of a Palladium Metallosquare with Encapsulated Fullerenes via Singlet Oxygen Generation, Inorg. Chem. 58 (2019) 11836-11842.
[87] E. Regulska, D. M. Rivera-Nazario, J. Karpinska, M. E. Plonska-Brzezinska, L. Echegoyen, Zinc Porphyrin-Functionalized Fullerenes for the Sensitization of Titania as a Visible-Light Active Photocatalyst: River Waters and Wastewaters Remediation, Molecules 24 (2019) 1118.
[88] A. Grebinyk, S. Prylutska, O. Chepurna, S. Grebinyk, Y. Prylutskyy, U. Ritter, T. Y. Ohulchanskyy, O. Matyshevska, T. Dandekar, M. Frohme, Synergy of Chemo- and Photodynamic Therapies with C_{60} Fullerene-Doxorubicin Nanocomplex, Nanomaterials 9 (2019) 1540.
[89] L. Xiao, R. Huang, Y. Zhang, T. Li, J. Dai, N. Nannapuneni, T. R. Chastanet, M. Chen, F. H.

Shen, L. Jin, H. C. Dorn, X. Li, A New Formyl Peptide Receptor-1 Antagonist Conjugated Fullerene Nanoparticle for Targeted Treatment of Degenerative Disc Diseases, ACS Appl. Mater. Interfaces 11 (2019) 38405-38416.
[90] A. Grebinyk, S. Prylutska, A. Buchelnikov, N. Tverdokhleb, S. Grebinyk, M. Evstigneev, O. Matyshevska, V. Cherepanov, Y. Prylutskyy, V. Yashchuk, A. Naumovets, U. Ritter, T. Dandekar, M. Frohme, C_{60} Fullerene as an Effective Nanoplatform of Alkaloid Berberine Delivery into Leukemic Cells, Pharmaceutics 11 (2019) 586.
[91] L. B. Sukhodub, L. F. Sukhodub, M. O. Kumeda, S. V. Prylutska, V. Deineka, Y. I. Prylutskyy, U. Ritter, C_{60} fullerene loaded hydroxyapatite-chitosan beads as a promising system for prolonged drug release, Carbohydr. Polym. 223 (2019) 115067.
[92] C. Guo, J. Chen, G. Li, X. Liang, W. Lai, L. Yang, Y. Mai, Z. Li, Enhanced Electrical Conductivity of Sb_2S_3 Thin Film via C_{60} Modification and Improvement in Solar Cell Efficiency, Global challenges 3 (2019) 1800108.
[93] T. Cao, K. Chen, Q. Chen, Y. Zhou, N. Chen, Y. Li, Fullerene Derivative-Modified SnO_2 Electron Transport Layer for Highly Efficient Perovskite Solar Cells with Efficiency over 21%, ACS Appl. Mater. Interfaces 11 (2019) 33825-33834.
[94] V. Arivazhagan, J. S. Xie, P. J. Hang, M. M. Parvathi, A. Khan, C. Cui, D. R. Yang, X. G. Yu, Interface engineering of C_{60}/fluorine doped tin oxide on the photovoltaic performance of perovskite solar cells using the physical vapor deposition technique, J. Phys. D Appl. Phys. 52 (2019) 225104.
[95] G. Li, S. Zheng, Exploring the effects of axial halogen substitutions of boron subphthalocyanines on the performance of BsubPC/C_{60} organic solar cells: a DFT/TDDFT-based computational study, New J. Chem. 43 (2019) 12719-12726.
[96] J. K. Roy, S. Kar, J. Leszczynski, Optoelectronic Properties of C_{60} and C_{70} Fullerene Derivatives: Designing and Evaluating Novel Candidates for Efficient P3HT Polymer Solar Cells, Materials 12 (2019) 2282.
[97] Q. Fu, S. Xiao, X. Tang, Y. Chen, T. Hu, Amphiphilic Fullerenes Employed to Improve the Quality of Perovskite Films and the Stability of Perovskite Solar Cells, ACS Appl. Mater. Interfaces 11 (2019) 24782-24788.
[98] L. Bai, Y. Chen, X. Liu, J. Zhou, J. Cao, L. Hou, S. Guo, Ultrasensitive electrochemical detection of Mycobacterium tuberculosis IS6110 fragment using gold nanoparticles decorated fullerene nanoparticles/nitrogen-doped graphene nanosheet as signal tags, Anal. Chim. Acta 1080 (2019) 75-83.
[99] D. Long, M. Li, H. Wang, H. Wang, Y. Chai, R. Yuan, A photoelectrochemical biosensor based on fullerene with methylene blue as a sensitizer for ultrasensitive DNA detection, Biosens. Bioelectron. 142 (2019) 111579.
[100] L. Shahhoseini, R. Mohammadi, B. Ghanbari, S. Shahrokhian, Ni(II) 1D-coordination polymer/C_{60}-modified glassy carbon electrode as a highly sensitive non-enzymatic glucose electrochemical sensor, Appl. Surf. Sci. 478 (2019) 361-372.
[101] L. Yang, X. Zhong, L. Huang, H. Deng, R. Yuan, Y. Yuan, C_{60}@C_3N_4 nanocomposites as quencher for signal-off photoelectrochemical aptasensor with Au nanoparticle decorated

perylene tetracarboxylic acid as platform, Anal. Chim. Acta 1077 (2019) 281-287.
[102] K. Lee, H. Song, J. T. Park, [60] Fullerene-metal cluster complexes: Novel bonding modes and electronic communication, Acc. Chem. Res. 36 (2003) 78-86.
[103] S. Bosi, T. Da Ros, G. Spalluto, M. Prato, Fullerene derivatives: an attractive tool for biological applications, Eur. J. Med. Chem. 38 (2003) 913-923.
[104] M. Saunders, R. J. Cross, H. A. Jimenez-Vazquez, R. Shimshi, A. Khong, Noble gas atoms inside fullerenes, Science 271 (1996) 1693-1697.
[105] D. M. Guldi, M. Prato, Excited-state properties of C_{60} fullerene derivatives, Acc. Chem. Res. 33 (2000) 695-703.
[106] V. Krishna, N. Noguchi, B. Koopman, B. Moudgil, Enhancement of titanium dioxide photocatalysis by water-soluble fullerenes, J. Colloid Interface Sci. 304 (2006) 166-171.
[107] V. Krishna, D. Yanes, W. Imaram, A. Angerhofer, B. Koopman, B. Moudgil, Mechanism of enhanced photocatalysis with polyhydroxy fullerenes, Appl. Catal. B Environ. 79 (2008) 376-381.
[108] Y. Park, N. J. Singh, K. S. Kim, T. Tachikawa, T. Majima, W. Choi, Fullerol-titania charge-transfer-mediated photocatalysis working under visible light, Chemistry 15 (2009) 10843-10850.
[109] J. Lee, Y. Mackeyev, M. Cho, L. J. Wilson, J.-H. Kim, P. J. J. Alvarez, C_{60} Aminofullerene Immobilized on Silica as a Visible-Light-Activated Photocatalyst, Environ. Sci. Technol. 44 (2010) 9488-9495.
[110] Z.-D. Meng, F.-J. Zhang, L. Zhu, C.-Y. Park, Trishs Ghosh, J.-G. Choi, W.-C. Oh Synthesis and characterization of M-fullerene/TiO_2 photocatalysts designed for degradation azo dye, Mater. Sci. Eng. C 32 (2012) 2175-2182.
[111] J. Lee, S. Hong, Y. Mackeyev, C. Lee, E. Chung, L. J. Wilson, J. H. Kim, P. J. Alvarez, Photosensitized oxidation of emerging organic pollutants by tetrakis C_{60} aminofullerene-derivatized silica under visible light irradiation, Environ. Sci. Technol. 45 (2011) 10598-10604.
[112] Y. Choi, Y. Ye, Y. Mackeyev, M. Cho, S. Lee, L. J. Wilson, J. Lee, P. J. J. Alvarez, W. Choi, J. Lee, C_{60} aminofullerene-magnetite nanocomposite designed for efficient visible light photocatalysis and magnetic recovery, Carbon 69 (2014) 92-100.
[113] Z. Meng, L. Zhu, J.-G. Choi, C.-Y. Park, W.-C. Oh, Rare Earth Oxide-Treated Fullerene and Titania Composites with Enhanced Photocatalytic Activity for the Degradation of Methylene Blue, Chin. J. Catal. 32 (2011) 1457-1464.
[114] E. M. Barker, J. P. Buchanan, Thiol-ene polymer microbeads prepared under high-shear and their successful utility as a heterogeneous photocatalyst via C_{60}-capping, Polymer 92 (2016) 66-73.
[115] Q. Chen, M. Q. Cheng, K. Yang, W. Q. Huang, W. Y. Hu, G. F. Huang, Dispersive and covalent interactions in all-carbon heterostructures consisting of penta-graphene and fullerene: topological effect, Journal of Physics D: Applied Physics 51 (2018) 305301.
[116] M. Grandcolas, J. H. Ye, K. Miyazawa, Titania nanotubes and fullerenes C_{60} assemblies and their photocatalytic activity under visible light, Ceram. Int. 40 (2014) 1297-1302.

[117] K. Kokubo, K. Matsubayashi, H. Tategaki, H. Takada, T. Oshima, Facile synthesis of highly water-soluble fullerenes more than half-covered by hydroxyl groups, ACS Nano 2 (2008) 327-333.
[118] J. P. Kamat, T. P. Devasagayam, K. I. Priyadarsini, H. Mohan, J. P. Mittal, Oxidative damage induced by the fullerene C_{60} on photosensitization in rat liver microsomes, Chem. Biol. Interact. 114 (1998) 145-159.
[119] J. Yu, T. Ma, G. Liu, B. Cheng, Enhanced photocatalytic activity of bimodal mesoporous titania powders by C_{60} modification, Dalton Trans. 40 (2011) 6635-6644.
[120] X. J. Ma, X. R. Li, M. M. Li, X. C. Ma, L. Yu, Y. Dai, Effect of the structure distortion on the high photocatalytic performance of C_{60}/g-C_3N_4 composite, Appl. Surf. Sci. 414 (2017) 124-130.
[121] J. G. Yu, T. T. Ma, G. Liu, B. Cheng, Enhanced photocatalytic activity of bimodal mesoporous titania powders by C_{60} modification, Dalton Trans. 40 (2011) 6635-6644.
[122] Z. Youssef, L. Colombeau, N. Yesmurzayeva, F. Baros, R. Vanderesse, T. Hamieh, J. Toufaily, C. Frochot, T. Roques-Carmes, S. Acherar, Dye-sensitized nanoparticles for heterogeneous photocatalysis: Cases studies with TiO_2, ZnO, fullerene and graphene for water purification, Dyes Pigment. 159 (2018) 49-71.
[123] Z. D. Meng, W. C. Oh, Support info of Photodegradation of Organic Dye by CoS_2 and Carbon(C_{60}, Graphene, CNT)/TiO_2 Composite Sensitizer, Chin. J. Catal. 33 (2012) 1495-1501.
[124] N. Justh, T. Firkala, K. Laszlo, J. Labar, I. M. Szilagyi, Photocatalytic C_{60}-amorphous TiO_2 composites prepared by atomic layer deposition, Appl. Surf. Sci. 419 (2017) 497-502.
[125] K. I. Katsumata, N. Matsushita, K. Okada, Preparation of TiO_2-Fullerene Composites and Their Photocatalytic Activity under Visible Light, Int. J. Photoenergy 2012 (2012) 256096.
[126] J. Lin, R. L. Zong, M. Zhou, Y. F. Zhu, Photoelectric catalytic degradation of methylene blue by C_{60}-modified TiO_2 nanotube array, Appl. Catal. B Environ. 89 (2009) 425-431.
[127] H. Fu, T. Xu, S. Zhu, Y. Zhu, Photocorrosion Inhibition and Enhancement of Photocatalytic Activity for ZnO via Hybridization with C_{60}, Environ. Sci.Technol. 42 (2008) 8064-8069.
[128] D. Ma, J. Zhong, R. Peng, J. Li, R. Duan, Effective photoinduced charge separation and photocatalytic activity of hierarchical microsphere-like C_{60}/BiOCl, Appl. Surf. Sci. 465 (2018) 249-258.
[129] G. D. Panagiotou, M. D. Tzirakis, J. Vakros, L. Loukatzikou, M. Orfanopoulos, C. Kordulis, A. Lycourghiotis, Development of [60] fullerene supported on silica catalysts for the photo-oxidation of alkenes, Appl. Catal. A General 372 (2010) 16-25.
[130] B. Chai, X. Liao, F. K. Song, H. Zhou, Fullerene modified C_3N_4 composites with enhanced photocatalytic activity under visible light irradiation, Dalton Trans. 43 (2014) 982-989.
[131] P. J. Krusic, E. Wasserman, B. A. Parkinson, B. Malone, E. R. Holler, Jr., P. N. Keizer, J. R. Morton, K. F. Preston, Electron spin resonance study of the radical reactivity of C_{60}, J. Am. Chem. Soc. 113 (1991) 6274-6275.
[132] J. W. Arbogast, A. P. Darmanyan, C. S. Foote, Y. Rubin, F. N. Diederich, M. M. Alvarez, S. J. Anz, R. L. Whetten, Photophysical properties of C_{60}, J. Phys. Chem. 95 (1991) 11-12.

[133] J. W. Arbogast, C. S. Foote, Photophysical properties of C_{70}, J. Am. Chem. Soc. 113 (1991) 8886-8889.
[134] J. Kyriakopoulos, A. T. Papastavrou, G. D. Panagiotou, M. D. Tzirakis, K. S. Triantafyllidis, M. N. Alberti, K. Bourikas, C. Kordulis, M. Orfanopoulos, A. Lycourghiotis, Deposition of fullerene C_{60} on the surface of MCM-41 via the one-step wet impregnation method: Active catalysts for the singlet oxygen mediated photooxidation of alkenes, J. Mol. Catal. A: Chem. 381 (2014) 9-15.
[135] P. V. Kamat, I. Bedja, S. Hotchandani, Photoinduced Charge Transfer between Carbon and Semiconductor Clusters. One-Electron Reduction of C_{60} in Colloidal TiO_2 Semiconductor Suspensions, J. Phys. Chem. 98 (1994) 9137-9142.
[136] V. I. Makarov, S. A. Kochubei, I. V. Khmelinskii, Photoconductivity of the TiO_2 +Fullerene-C_{60} bilayers: steady-state and time-resolved measurements, Chem. Phys. Lett. 355 (2002) 504-508.
[137] Z.-D. Meng, L. Zhu, J.-G. Choi, M.-L. Chen, W.-C. Oh, Effect of Pt treated fullerene/TiO_2 on the photocatalytic degradation of MO under visible light, J. Mater. Chem. 21 (2011) 7596-7603.
[138] T. Song, J. Huo, T. Liao, J. Zeng, J. Y. Qin, H. Zeng, Fullerene [C_{60}] modified $Cr_{2-x}Fe_xO_3$ nanocomposites for enhanced photocatalytic activity under visible light irradiation, Chem. Eng. J. 287 (2016) 359-366.
[139] Z. C. Lian, P. P. Xu, W. C. Wang, D. Q. Zhang, S. N. Xiao, X. Li, G. S. Li, C_{60}-Decorated CdS/TiO_2 Mesoporous Architectures with Enhanced Photostability and Photocatalytic Activity for H_2 Evolution, ACS Appl. Mater. Interfaces 7 (2015) 4533-4540.
[140] J. Kyriakopoulos, M. D. Tzirakis, G. D. Panagiotou, M. N. Alberti, K. S. Triantafyllidis, S. Giannakaki, K. Bourikas, C. Kordulis, M. Orfanopoulos, A. Lycourghiotis, Highly active catalysts for the photooxidation of organic compounds by deposition of [60] fullerene onto the MCM-41 surface: A green approach for the synthesis of fine chemicals, Appl. Catal. B Environ. 117 (2012) 36-48.
[141] W. Ryo, K. Tamako, I. Fuyu, U. Hisanao, M. Hiroshi, Decomposition of methyl orange using C_{60} fullerene adsorbed on silica gel as a photocatalyst via visible-light induced electron transfer, Appl. Catal. B Environ. 166-167 (2015) 544–550.
[142] Z. D. Meng, L. Zhu, K. Ullah, S. Ye, W. C. Oh, Detection of oxygen species generated by WO_3 modification fullerene/TiO_2 in the degradation of 1,5-diphenyl carbazide, Mater. Res. Bull. 56 (2014) 45-53.
[143] L. T. Ju, P. X. Wu, Q. L. Yang, Z. Ahmed, N. W. Zhu, Synthesis of ZnAlTi-LDO supported C_{60}@AgCl nanoparticles and their photocatalytic activity for photo-degradation of Bisphenol A, Appl. Catal. B Environ. 224 (2018) 159-174.
[144] Z. J. Du, W. Z. Li, Z. P. Xu, H. Wu, H. Jameel, H. M. Chang, L. L. Ma, Characterization Of $C_{60}/Bi_2TiO_4F_2$ as a Potential Visible Spectrum Photocatalyst for The Depolymerization of Lignin, J. Wood Chem. Technol. 36 (2016) 365-376.
[145] S. Cao, J. Yu, Carbon-based H_2-production photocatalytic materials, J. Photochem. Photobiol. C-Photochem. Rev. 27 (2016) 72-99.

[146] J. X. Low, J. G. Yu, M. Jaroniec, S. Wageh, A. A. Al-Ghamdi, Heterojunction Photocatalysts, Adv. Mater. 29 (2017) 1601694.
[147] P. Zhou, J. Yu, M. Jaroniec, All-Solid-State Z-Scheme Photocatalytic Systems, Adv. Mater. 26 (2014) 4920-4935.
[148] E. Kanchanatip, N. Grisdanurak, R. Thongruang, A. Neramittagapong, Degradation of paraquat under visible light over fullerene modified V-TiO_2, React Kinet Mech Cat 103 (2011) 227-237.
[149] S. Deguchi, S. Mukai, M. Tsudome, K. Horikoshi, Facile generation of fullerene nanoparticles by hand-grinding, Adv. Mater. 18 (2006) 729-732.
[150] S. Deguchi, R. G. Alargova, K. Tsujii, Stable dispersions of fullerenes, C_{60} and C_{70}, in water. Preparation and characterization, Langmuir 17 (2001) 6013-6017.
[151] A. Hirsch, The Chemistry of the Fullerenes: An Overview, Angew. Chem. Int. Ed. 32 (1993) 1138-1141.
[152] M. Dallavalle, M. Leonzio, M. Calvaresi, F. Zerbetto, Explaining Fullerene Dispersion by using Micellar Solutions, Chemphyschem 15 (2014) 2998-3005.
[153] V. M. Torres, M. Posa, B. Srdjenovic, A. L. Simplicio, Solubilization of fullerene C_{60} in micellar solutions of different solubilizers, Colloids and surfaces. B, Biointerfaces 82 (2011) 46-53.
[154] D. Canevet, E. M. Perez, N. Martin, Wraparound Hosts for Fullerenes: Tailored Macrocycles and Cages, Angew. Chem. Int. Ed. 50 (2011) 9248-9259.
[155] L. Moreira, J. Calbo, R. M. K. Calderon, J. Santos, B. M. Illescas, J. Arago, J. F. Nierengarten, D. M. Guldi, E. Orti, N. Martin, Unveiling the nature of supramolecular crown ether-C_{60} interactions, Chem. Sci. 6 (2015) 4426-4432.
[156] M. Di Giosia, P. H. H. Bomans, A. Bottoni, A. Cantelli, G. Falini, P. Franchi, G. Guarracino, H. Friedrich, M. Lucarini, F. Paolucci, S. Rapino, N. Sommerdijk, A. Solda, F. Valle, F. Zerbetto, M. Calvaresi, Proteins as supramolecular hosts for C_{60}: a true solution of C_{60} in water, Nanoscale 10 (2018) 9908-9916.
[157] V. Apostolopoulou, J. Vakros, C. Kordulis, A. Lycourghiotis, Preparation and characterization of [60] fullerene nanoparticles supported on titania used as a photocatalyst, Colloids and Surfaces A: Physicochem. Eng. Aspects 349 (2009) 189-194.
[158] J. Kyriakopoulos, E. Kordouli, K. Bourikas, C. Kordulis, A. Lycourghiotis, Decolorization of Orange-G Aqueous Solutions over C_{60}/MCM-41 Photocatalysts, Appl. Sci.-Basel 9 (2019) 1958.
[159] T. Y. Xu, R. L. Zhu, J. X. Zhu, X. L. Liang, G. Q. Zhu, Y. Liu, Y. Xu, H. P. He, Fullerene modification of Ag_3PO_4 for the visible-light-driven degradation of acid red 18, RSC Adv. 6 (2016) 85962-85969.
[160] C.-Y. Zou, Z.-D. Meng, W.-C. Ji, S.-Q. Liu, Z. Shen, Y. Zhang, N.-S. Jiang, Preparation of a fullerene [60] -iron oxide complex for the photo-fenton degradation of organic contaminants under visible-light irradiation, Chin. J. Catal. 39 (2018) 1051-1059.
[161] M. D. Tzirakis, J. Vakros, L. Loukatzikou, V. Amargianitakis, M. Orfanopoulos, C. Kordulis, A. Lycourghiotis, γ-Alumina-supported [60]fullerene catalysts: Synthesis, properties

and applications in the photooxidation of alkenes, J. Mol. Catal. A: Chem. 316 (2010) 65-74.
[162] M. E. Navgire, M. K. Lande, Effect of nanocrystalline composite fullerene-doped MoO_3-TiO_2 material on photoassisted degradation of Alizarin red S dye, Inorganic and Nano-Metal Chemistry 47 (2017) 320-327.
[163] X. Lin, R. Zhao, Y. Xi, X. Li, J. Shi, N. Yan, Metal-free C_{60}/CNTs/g-C_3N_4 ternary heterostructures: synthesis and enhanced visible-light-driven photocatalytic performance, R .Soc. Open Sci. 5 (2018) 172290.
[164] L. M. Song, C. P. Guo, T. T. Li, S. J. Zhang, C_{60}/graphene/g-C_3N_4 composite photocatalyst and mutually- reinforcing synergy to improve hydrogen production in splitting water under visible light radiation, Ceram. Int. 43 (2017) 7901-7907.
[165] M. B. Tahir, G. Nabi, M. Rafique, N. R. Khalid, Role of fullerene to improve the WO_3 performance for photocatalytic applications and hydrogen evolution, Int. J. Energy Res. 42 (2018) 4783-4789.
[166] X. Zhao, H. Liu, Y. Shen, J. Qu, Photocatalytic reduction of bromate at C_{60} modified Bi_2MoO_6 under visible light irradiation, Appl. Catal. B Environ. 106 (2011) 63-68.
[167] K. Qi, R. Selvaraj, T. Al Fahdi, S. Al-Kindy, Y. Kim, G. Wang, C. W. Tai, M. Sillanpaa, Enhanced photocatalytic activity of anatase-TiO_2 nanoparticles by fullerene modification: A theoretical and experimental study, Appl. Surf. Sci. 387 (2016) 750-758.
[168] G. Li, B. Jiang, X. Li, Z. Lian, S. Xiao, J. Zhu, D. Zhang, H. Li, C_{60}/$Bi_2TiO_4F_2$ Heterojunction Photocatalysts with Enhanced Visible-Light Activity for Environmental Remediation, ACS Appl. Mater. Interfaces 5 (2013) 7190-7197.
[169] S. Zhu, T. Xu, H. Fu, J. Zhao, Y. Zhu, Synergetic effect of Bi_2WO_6 photocatalyst with C_{60} and enhanced photoactivity under visible irradiation, Environ. Sci. Technol. 41 (2007) 6234-6239.
[170] Y. X. Wei, M. G. Ma, W. L. Li, J. Yang, H. Miao, Z. J. Zhang, Y. F. Zhu, Enhanced photocatalytic activity of PTCDI-C_{60} via pi-pi interaction, Appl. Catal. B Environ. 238 (2018) 302-308.
[171] Y. Zhu, M. Laipan, R. Zhu, T. Xu, J. Liu, J. Zhu, Y. Xi, G. Zhu, H. He, Enhanced photocatalytic activity of Zn/Ti-LDH via hybridizing with C_{60}, J. Mol. Catal. A: Chem. 427 (2017) 54-61.
[172] X. Chen, H. Chen, J. Guan, J. Zhen, Z. Sun, P. Du, Y. Lu, S. Yang, A facile mechanochemical route to a covalently bonded graphitic carbon nitride (g-C_3N_4) and fullerene hybrid toward enhanced visible light photocatalytic hydrogen production, Nanoscale 9 (2017) 5615-5623.
[173] A. Behera, S. Mansingh, K. K. Das, K. Parida, Synergistic $ZnFe_2O_4$-carbon allotropes nanocomposite photocatalyst for norfloxacin degradation and Cr(VI) reduction, J. Colloid Interface Sci. 544 (2019) 96-111.
[174] H. S. Park, W. B. Ko, Preparation of C_{60} Nanowhiskers-SnO_2 Nanocomposites and Photocatalytic Degradation of Organic Dyes, J. Nanosci. Nanotechno. 15 (2015) 8125-8132.
[175] K. Shahzad, M. B. Tahir, M. Sagir, Engineering the performance of heterogeneous WO_3/fullerene@Ni_3B/$Ni(OH)_2$ Photocatalysts for Hydrogen Generation, Int. J. Hydrogen

Energy 44 (2019) 21738-21745.
[176] Y. Long, Y. Lu, Y. Huang, Y. Peng, Y. Lu, S. Kang, J. Mu, Effect of C_{60} on the Photocatalytic Activity of TiO_2 Nanorods, J. Phys. Chem. C 113 (2009) 13899-13905.
[177] R. Buonsanti, V. Grillo, E. Carlino, C. Giannini, T. Kipp, R. Cingolani, P. D. Cozzoli, Nonhydrolytic synthesis of high-quality anisotropically shaped brookite TiO_2 nanocrystals, J. Am. Chem. Soc. 130 (2008) 11223-11233.
[178] W. Oh, F. Zhang, M. Chen, Synthesis and characterization of V-C_{60}/TiO_2 photocatalysts designed for degradation of methylene blue, J. Ind. Eng. Chem. 16 (2010) 299-304.
[179] Z. Liu, Y. Liu, G. Zeng, B. Shao, M. Chen, Z. Li, Y. Jiang, Y. Liu, Y. Zhang, H. Zhong, Application of molecular docking for the degradation of organic pollutants in the environmental remediation: A review, Chemosphere 203 (2018) 139-150.
[180] S. Ding, W. Huang, B. Zhou, P. Peng, W. Hu, M. Long, G. Huang, The mechanism of enhanced photocatalytic activity of SnO_2 through fullerene modification, Curr. Appl. Phys. 17 (2017) 1547-1556.
[181] L. Zhang, Y. Wang, T. Xu, S. Zhu, Y. Zhu, Surface hybridization effect of C_{60} molecules on TiO_2 and enhancement of the photocatalytic activity, J. Mol. Catal. A: Chem. 331 (2010) 7-14.
[182] K. J. Moor, J. H. Kim, Simple Synthetic Method Toward Solid Supported C_{60} Visible Light-Activated Photocatalysts, Environ. Sci. Technol. 48 (2014) 2785-2791.
[183] L. Brunet, D. Y. Lyon, E. M. Hotze, P. J. J. Alvarez, M. R. Wiesner, Comparative Photoactivity and Antibacterial Properties of C_{60} Fullerenes and Titanium Dioxide Nanoparticles, Environ. Sci. Technol. 43 (2009) 4355-4360.
[184] Y. Jiang, Z. Liu, G. Zeng, Y. Liu, B. Shao, Z. Li, Y. Liu, W. Zhang, Q. He, Polyaniline-based adsorbents for removal of hexavalent chromium from aqueous solution: a mini review, Environ. Sci. Pollut. Res. 25 (2018) 6158-6174.
[185] Y. Liu, Z. Liu, G. Zeng, M. Chen, Y. Jiang, B. Shao, Z. Li, Y. Liu, Effect of surfactants on the interaction of phenol with laccase: Molecular docking and molecular dynamics simulation studies, J. Hazard. Mater. 357 (2018) 10-18.
[186] Z. Liu, M. Yu, G. Zeng, M. Li, J. Zhang, H. Zhong, Y. Liu, B. Shao, Z. G. Li, Z. Wang, G. Liu, X. Yang, Investigation on the reaction of phenolic pollutions to mono-rhamnolipid micelles using MEUF, Environ. Sci. Pollut. Res. 24 (2017) 1230-1240.
[187] Z. Liu, B. Shao, G. Zeng, M. Chen, Z. Li, Y. Liu, Y. Jiang, H. Zhong, Y. Liu, M. Yan, Effects of rhamnolipids on the removal of 2,4,2,4-tetrabrominated biphenyl ether (BDE-47) by Phanerochaete chrysosporium analyzed with a combined approach of experiments and molecular docking, Chemosphere 210 (2018) 922-930.
[188] Q. Li, L. Xu, K. W. Luo, W. Q. Huang, L. L. Wang, X. F. Li, G. F. Huang, Y. B. Yu, Insights into enhanced visible-light photocatalytic activity of C_{60} modified g-C_3N_4 hybrids: the role of nitrogen, Phys. Chem. Chem. Phys. 18 (2016) 33094-33102.
[189] J. P. Huo, H. P. Zeng, A novel triphenylamine functionalized bithiazole-metal complex with C_{60} for photocatalytic hydrogen production under visible light irradiation, J. Mater. Chem. A 3 (2015) 6258-6264.

[190] B. Chai, T. Y. Peng, X. H. Zhang, J. Mao, K. Li, X. G. Zhang, Synthesis of C_{60}-decorated SWCNTs (C_{60}-d-CNTs) and its TiO_2-based nanocomposite with enhanced photocatalytic activity for hydrogen production, Dalton Trans. 42 (2013) 3402-3409.